

## Report #1

### Author general comment

*We would like to thank the reviewer for reviewing manuscript "ICME impact at Earth with low and typical Mach number plasma characteristics" and thus helping to improve it. We considered carefully every comment made by the reviewer and prepared responses accordingly. Please find our responses to the comments below.*

---

## General comments

---

Reviewer report on paper "ICME impact at Earth with low and typical Mach number plasma characteristics" by Antti Lakka et al. The authors present their analysis of global MHD (GUMICS model) simulations of solar wind-magnetosphere-ionosphere system during two interplanetary cloud events. They compute the magnetopause standoff distance and magnetic fields along the trajectories of magnetospheric spacecraft (and compare them to empirical models and spacecraft observations), estimate approximately the amount of energy transferred into the magnetosphere, and analyse the potential drop applied in the ionosphere (CPCP) which characterizes the intensity of global convection.

The main problem for me with this paper is that it actually tries to address two related problems, physical effects (ICME impact differences, e.g. saturation) and technical aspects (validation of GUMICS computation results). Second aspect is crucial because, if the computed values are wrong and do not characterize the reality, they can not be used to study the physics in the magnetospheric system. Unfortunately in the paper only the first problem is formally claimed as a paper goal: all Introduction, the paper title and most of the abstract are about the properties of ICME. As concerns the results - the only ICME-related conclusion (last line in the Abstract) is that 'CPCP saturation is affected by the upstream conditions, with strong dependence on the Alfvén Mach number'. In such formulation this is actually well-known from many previous studies, including simulations. So - no new results??

*We thank the reviewer for this comment. It forced us to rethink what we want to say in the paper and obtained new results. The leading thought of the paper is to 1) consider two different ICME events and observe if they produce different effects on the magnetospheric physics by considering several parameters and 2) assess how GUMICS-4 reproduces those events by providing an uncertainty estimate with every parameter. We e.g. show that the accuracy of GUMICS-4 results is dependent on the magnetospheric region under inspection. We have now improved the exposure of the technical aspects starting from abstract and introduction (see pages 1 and 3).*

My impression is that throughout the paper the authors are under a strong pressure of technical aspects because the GUMICS validation results are not very optimistic: the B-field comparisons demonstrate big differences between the predictions and observations (whose origin is not identified); the computed CPCP values are much lower than usual ones; their values differ significantly between two simulation runs at standard and doubled resolution, and there is no confidence that the high-resolution run reached the optimum (CPCP values are still low to my view). No clear conclusions about validation success were done in the discussion/conclusion sections.

***We agree with the reviewer in the sense that GUMICS-4 produces different results when compared with e.g. in-situ satellite observations or measured polar cap potential. It is not even a surprise, since there have been many studies before reporting how well GUMICS-4 (or any other global MHD code) captures the magnetospheric dynamics. The problem is partly due to MHD physics not being sufficient, but also partly because the compared quantities may not represent the same quantities at all. For instance, a corresponding observation for global MHD CPCP is hard to find. Some studies have used PCN index, which doesn't really represent a global CPCP value. Others have used potentials deduced from ionospheric radars, but still do not capture the entire polar cap area. Given these difficulties in the validation, our best approach is to use well-known references, validate simulation results, report the shortcomings of our validation, and assess how well we succeeded. This is just what we do in our paper and we hope that it is now easier to see especially in the discussion and conclusion sections of the revised manuscript.***

A big general problem with GMHD simulations is that, for the same solar wind inputs, different GMHD models (their runs at comparable resolution) provide very different answers for essential output parameters (incl. global parameters) –see Gordeev et al. (Space Weather 2015, 2017). For some parameters like the MP standoff distance, the deviations between models were not large. For some other parameters like CPCP and total field-aligned current, their values differ greatly between models, with GUMICS showed too low values of both global variables. This problem is not distinctly articulated in the paper, although a common need of truly global and accurate simulation models justifies paying attention to the technical (validation) aspects as well.

***Different GMHD models have different strengths. Deviations in e.g. CPCP values are caused by differences in how the models handle excessive amount of electric current through the polar cap, which causes some models to underestimate, others to overestimate CPCP. Using GMHD model requires knowledge of the general features of the model performance and understanding their strengths and limitations. Shedding light to this issue is one of the key targets of this paper. From our paper point of view, comparing the time evolution of e.g. CPCP between GUMICS-4 and reference parameter is important. This aspect is articulated better in the revised manuscript.***

In view of these problems, I believe, the paper in the existing form can not be recommended to the publication. However, I believe, the authors still have potentially interesting material in hands and can possibly find a proper balance between two (physical and technical) aspects to reorganize the manuscript, to clearly formulate and answer the main questions to be addressed, and to expose the new results as a response to the formulated goals (not necessarily being all positive????).

---

### **Specific comments**

---

p.3 - 1.3 to7: Paper goal is not actually explained, you only tell that you do simulations during two ICME events and compute magnetopause, but not – which problem are you focusing on in that paper? What drives your choice of computed characteristics (MP distance, energy input, magnetic fields, . . . , how it helps to reach the goal?

***We agree with the reviewer. Those parameters are used because they are strongly affected by (especially strong) ICME events. The goal of this paper is to see how the parameters are affected by ICMEs with different strength AND how accurate GUMICS-4 results are in those (ICME) conditions. To achieve our goal, we use those parameters and compare***

***simulation results with known references and compute uncertainty estimate. The end of the introduction section hopefully highlights these issues better now. Please see page 3.***

Figs.1,2: The energetic particle fluxes are not used in the study??? Why don't use logarithmic scale for MA, otherwise the values in the most interesting small MA region are not readable from the plot

***We thank the reviewer for this comment. We adopted logarithmic scale for MA since it really makes figs 1,2 a lot better. However, even if energetic particle fluxes are not directly used in the study, showing them along with solar wind data provides additional information in a sense that it verifies magnetic cloud onset time especially for the 2012 event; gradual decrease of proton flux is observed at the same time with solar wind density decrease. On the other hand, absence of such flux decrease in 2014 shows that the event truly is moderate compared with the 2012 event.***

p.5, comparison of magnetic fields in the magnetosphere. First, it would be natural to place comparison of simulated/observed fields at the end of this paragraph where you show the results, otherwise (as it is now) the discussion of comparisons (now placed in sect.4.3) stays couple pages later from the corresponding figure, very hard to read.

***We think that the actual results are better to be found in the same section (Analysis) together with global dynamics results. Otherwise we would have to choose which results we are reporting in section 3 already (just measured Bmag or GUMICS-4 Bmag as well, what about the relative differences shown in the revised figures 4 and 5?)***

p.6-26:” Total energy through the dayside magnetopause is computed by evaluating the Poynting flux in the vicinity of the (Shue) magnetopause, and its component parallel to the magnetopause surface normal.” Your method to compute the energy flow is not sufficiently introduced and analysed, although there are big questions. The Shue magnetopause stays at some distance from simulated MP, in the region with large spatial gradients of flow and other parameters; also, the shapes of computed and Shue magnetopauses can be different. That means some portions of Shue MP can be in the magnetosheath (with tailward energy flow), some in the magnetosphere (with sunward Poynting flux near the dayside MP). How can you justify your computations? One way to quickly look on that is to compute energy flows throughout Shue MPs displaced, say by  $dX = +/-0.2$  (or  $0.5$ ) $R_E$ . Anyway, the uncertainty of such computations should be somehow estimated.

***We provide detailed explanation of the used method in the revised manuscript. It is true that the shape of the Shue magnetopause probably differs from the actual magnetopause. Previously, Palmroth et. al. (doi:10.1029/2002JA009446) computed the shape of actual magnetopause from GUMICS-4 results and compared energy transfer to the epsilon parameter. They also showed that the energy perpendicular to the boundary did not change with small displacement of the boundary thus demonstrating the robustness of the method to calculate the incoming energy. Instead, we consider the Shue magnetopause surface by displacing its nose 30% Sunward. We use 30% since it is maximum relative difference in magnetopause position between GUMICS-4 and the Shue model. This prevents underestimation of the size of the magnetosphere. The method used here gives values for energy of the same order of magnitude compared to study by Palmroth (mentioned above). Thus, we have good confidence in the methodology. See pages 8-9.***

pp.6-7: When validating MP and CPCP it would be reasonable to compare with empirical values for those conditions. I would also recommend to compare your results with Gordeev et al.(2015, doi:10.1002/2015SW001307) validation effort, where the empirical data have been used for testing (e.g., their Fig.9).

***We agree. In order to be consistent when using references, we have compared MP, energy transfer and CPCP to known references. For MP the reference is the Shue model, for energy transfer it's the epsilon parameter, and for the CPCP it is PCI (Ridley, Polar cap index comparisons with AMIE cross polar cap potential, electric field, and polar cap area, (2004)) deduced from PNC index. All of these have been used in previous studies and are easy to plot alongside GUMICS-4 results. Comparisons to PCI and epsilon were missing from the previous manuscript version, but are added in the revised version (see figures 6 and 7 and section 4.1). Moreover, we provide a framework to our study by comparing our results to work by Gordeev (see Discussion section).***

Section 4.3.Local dynamics. I think, a so big difference of magnitudes between GUMICS predictions and actual observations in Figs.4,5, a two-fold differences (or more) in many regions, is a kind of bad news for GUMICS validation. However- no analyses is provided – what was wrong in simulated field in these regions? How much the total pressure is wrong? Which components are most affected, etc?? Why don't you show the traces of high-resolution run results on Figs.4,5, are there differences between two runs? I don't see any conclusions from these comparisons, it may not be a good idea to show such bad agreement without explanations.

***We agree. The discussion of the results in this section is now improved. We show that accuracy of GUMICS-4 is dependent on which part of the magnetosphere is considered. The absolute value of Bmag in GUMICS-4 agrees better when Bmag is high (S/C is close to the Earth).***

An interesting aspect: if the saturation works under total FAC being an order of magnitude smaller than real , it may show that magnetospheric mechanisms (e.g. the FAC influence on the dayside magnetospheric magnetic field as suggested by G.Siscoe et al) do not contribute to the saturation effect. This can be a useful side result in case if your high resolution is not yet sufficient to increase CPCP and total FAC toward realistic values..

***Thank you for this comment. We considered it carefully in the text.***

---

## Report #2

### Author general comment

*We would like to thank the reviewer for reviewing manuscript "ICME impact at Earth with low and typical Mach number plasma characteristics" and thus helping to improve it. We considered carefully every comment made by the reviewer and prepared responses accordingly. Please find our responses to the comments below.*

---

### General comments

---

This paper studies the effect of two ICMEs of different characteristics on the Earth's magnetosphere, focussing on the saturation of the cross polar cap potential (CPCP). The majority of the abstract talks about the properties of the ICMEs, and is lacking in actual results, or the motivation of the paper. The introduction has a good overview of the relevant literature.

However, like the abstract, it is missing the aims and motivation of the paper. Whilst the results are interesting, I have concerns about their validity. The validation performed in the paper is minimal, only comparing simulation to spacecraft magnetic field data and the position of the magnetopause with the Shue model.

*We thank the reviewer for this comment. The manuscript is revised carefully to increase the amount of validation. Every parameter considered comes now with validation. Based on this, conclusions are also made of the accuracy of GUMICS-4 results.*

The comparison with spacecraft data is missing a key aspect, the plasma data, and there is little explanation for why GUMICS-4 underestimates the magnetic field strength.

*While the plasma motions are critically important, in this case it is not easy due to the fact that the S/C reside most of the time in the low-density lobe regions, where the observations suffer from the very low counts. Furthermore, there are large data gaps in the observations hindering the comparisons.*

The comparison of the Shue model with the simulation magnetopause is also missing key details, such as the definition of the "dayside magnetopause" and whether errors include the full 3D simulation magnetopause. A two or three dimensional comparison would be more appropriate.

*The Shue magnetopause nose position is a single grid point in GUMICS-4 results. This is explained in the revised manuscript. See page 7, line 29. Similarly, the dayside magnetopause is a 3D surface computed from its nose position, extending from 0 RE in Sunward direction. See page 7.*

This leads to the other issue with the paper, the calculation of the total energy into the magnetosphere. The Shue model is an axisymmetric model, and does not include features such as the cusps, hence using the Shue model for this calculation is potentially incorrect, capturing the sheath or magnetosphere.

*When computing the 3D Shue magnetopause for evaluating the amount of transferred energy, we have displaced its nose position by 30% Sunward to avoid inclusion of*

***magnetosphere. The methods are explained in detail in the revised manuscript. Moreover, earlier studies have demonstrated the robustness of the energy computations (Palmroth et al. (doi:10.1029/2002JA009446)). See pages 8-9.***

The overall quality of the writing in the paper is adequate with a few spelling, grammatical and citation style errors. These have been pointed out in the specific and technical comments, though the authors should thoroughly proof read. Though the results are interesting, I would not recommend the paper for publication in its current form. However, with a little more analysis and responding of the questions posed in this review, it has the potential for publication.

---

### **Specific comments**

---

- Pg 3, Section 2.1: Do you consider a dipole tilt or rotation? This should be stated

***We agree. Dipole field was rotating and the angle was nonzero. This is explained in the revised manuscript (see page 4).***

- Pg 4, Ln 14: You should be specific in why it's not feasible. Does it run too slowly, or are there memory issues?

***Simulations would take way too much time, probably months. In the revised manuscript we state that "...not feasible due to long simulation physical time (up to 3.5 days) and resulting long simulation running times." (see page 4).***

- Pg 4, Ln 11: Should list the solar wind values you're referencing to make it easier to understand

***We agree. The used solar wind values are listed in the revised manuscript. (see page 4).***

- Pg 6, Ln 26: Why do you use the Shue magnetopause for this calculation, not the simulation magnetopause? I would have thought this would be a more consistent calculation with the simulation. The general 3D structure of the Shue magnetopause likely not in the correct position, especially near the cusps. Does this mean you'd be capturing energy flux through an arbitrary surface either in the sheath or inside the magnetopause? Also, does this use the 3D magnetopause surface and how far does the dayside region extend to? The details of this calculation should be more clearly stated in the paper (or cited).

***We thank the reviewer for this comment. Previously, Palmroth et al. (doi:10.1029/2002JA009446) computed the shape of actual magnetopause from GUMICS-4 results and compared energy transfer to epsilon parameter. They also showed that the energy perpendicular to the boundary did not change with small displacement of the boundary thus demonstrating the robustness of the method to calculate the incoming energy. Instead, we consider the dayside (extends to 0 RE) Shue magnetopause 3D surface by displacing its nose 30% Sunward. We use 30% since it is maximum relative difference in magnetopause position between GUMICS-4 and the Shue model. This prevents underestimation of the size of the magnetosphere. The method used here gives values for energy of the same order of magnitude compared to study by Palmroth (mentioned above). Thus, we have good confidence in the methodology. We provide detailed explanation of the used method in the revised manuscript. See pages 8-9.***

- Pg 7, Lns 1-5: Continuing on from the previous comment, are these percentages over the whole 3D dayside surface of the magnetopause? If they aren't then they probably aren't a good metric as they don't account for the full shape of the magnetopause.

***The percentages are for the nose position. As the 3D Shue magnetopause structure is characterized by the position of the nose, we (and several other authors whose work we cite) strongly believe that this gives a good overview of the accuracy of the GUMICS-4 magnetopause position. Different models (empirical and simulations) produce different flaring in the distant magnetotail, but mostly agree within the dayside and near-tail region. Thus, considering the entire magnetopause Sunward of -30 RE would lead to similar conclusions. We do mention several times in the text that we only consider magnetopause nose to make that point clear.***

- Pg 7, Ln 10: The author mentions both runs are consistent; this should be shown with a figure of the GUMICS magnetosphere data (e.g. cuts through the noon-midnight and ecliptic planes).

***We agree. However, as section 4.1 is revised, the paragraph in question is not relevant anymore and has been removed.***

- Fig 4c: What is the strange artefact in the position of Geotail? It seems to jump to a different position?

***The artefacts are errors made when interpolating SC location over data gaps. These errors are removed from the revised figure 4.***

- Fig. 5: More odd artefacts: (c) position of geotail jumps throughout dataset; (b) jumps in the magnetic field strength of Cluster at approx. April 30 (06:00) and April 30 (09:00)

***Regarding (c): Also interpolation error, which does not show in the revised version of figure 5. Regarding (b): The measured Bmag increases from approx. 10 nT to 30 nT, which is on par with the increase of measured Bmag at 12:00 (April 30). At same time the magnetopause is in motion toward the Earth, and the S/C resides close to it, which probably explains those rapid increases.***

---

## **Technical comments**

---

- Pg 4, Ln 10: Need brackets around Lakka et al. (2017)

***Corrected in the revised manuscript. See page 4.***

- Pg 5 Ln 6: “rotate”, not “rotated”

***Corrected in the revised manuscript. See page 5.***

- Pg 5, Ln 30: Citation should have parentheses

***Corrected in the revised manuscript. See page 6.***

- Pg 6, Ln 11: replace “proper” with “properly”

***Word “proper” is referring to the “actual” part of the magnetic cloud, and that’s why we think that its usage in the context of the text is justifiable.***

- Fig 8. Ln 4: replace “are showing” with “show”

***Corrected in the revised manuscript. See figure 8 caption.***

- Pg 10: Ln 2: unnecessary hyphen in front of “line”

***Corrected in the revised manuscript. See page 11.***

- Pg 10, Ln 8: Citation should not have parentheses

***Corrected in the revised manuscript. See page 11.***

- Pg 10, Ln 20: Citation should have parentheses

***Corrected in the revised manuscript. See page 12.***

- Pg 11, Ln 14: Citation should have parentheses

***Corrected in the revised manuscript. See page 13.***

# ICME impact at Earth with low and typical Mach number plasma characteristics

Antti Lakka<sup>1</sup>, Tuija I. Pulkkinen<sup>1,6</sup>, Andrew P. Dimmock<sup>2</sup>, Emilia Kilpua<sup>3</sup>, Matti Ala-Lahti<sup>3</sup>, Ilja Honkonen<sup>4</sup>, Minna Palmroth<sup>3</sup>, and Osku Raukunen<sup>5</sup>

<sup>1</sup>Department of Electronics and Nanoengineering, Aalto University, Finland

<sup>2</sup>Swedish Institute of Space Physics, Uppsala, Sweden

<sup>3</sup>Department of Physics, University of Helsinki, Helsinki, Finland

<sup>4</sup>Finnish Meteorological Institute, Helsinki, Finland

<sup>5</sup>Department of Physics and Astronomy, University of Turku, Turku, Finland

<sup>6</sup>University of Michigan, Ann Arbor, USA

**Correspondence:** Antti Lakka (antti.lakka@aalto.fi)

## Abstract.

We study how the the Earth's magnetosphere responds to the fluctuating solar wind conditions caused by ~~two different~~ ~~amplitude~~ interplanetary coronal mass ejection (ICME) events by using the Grand Unified Magnetosphere-Ionosphere Coupling Simulation (GUMICS-4). ~~ICME events are known to drive strong geomagnetic disturbances and thus generate conditions~~ ~~that may lead to saturation of the cross-polar cap potential (CPCP).~~ The two ICME events occurred on 15–16 July 2012 and 29–30 April 2014. During the 2012 event, the solar wind upstream values reached up to 35 particles/cm<sup>3</sup>, speed of 694 km/s, and interplanetary magnetic field of 22 nT. The event of 2014 was a moderate one, with the corresponding upstream values of 30 particles/cm<sup>3</sup>, 320 km/s and 10 nT. The mean upstream Alfvén Mach number was 2.3 for the 2012 event, while it was 5.8 for the 2014 event. We examine how the Earth's space environment dynamics evolves during both ICME events covering both global and local perspectives, including saturation of the cross-polar cap potential CPCP. To validate the accuracy of the GUMICS-4 simulation we use well-established references, such as the Shue model, and satellite data from ~~several missions~~ ~~located in~~ different parts of the magnetosphere. ~~It is shown that the CPCP saturation is affected by the upstream conditions, with strong dependence.~~ We show that in the large scale, and during moderate driving, the GUMICS-4 results are in good agreement with the reference values. However, the local values, especially during high driving, show more variation. The CPCP saturation depends on one hand on the simulation resolution, and on the other hand on the Alfvén Mach number of the upstream solar wind.

## 1 Introduction

~~According to the present understanding,~~ Present understanding is that the coupling of the solar wind and the Earth's magnetosphere ~~is conducted by~~ occurs via magnetic reconnection (Dungey, 1961) and viscous processes (Axford and Hines, 1961) such as the Kelvin-Helmholtz instability (e.g. Nykyri and Otto (2001)) and diffusion (Johnson and Cheng, 1997). Although viscous processes may play a strong role, particularly when the interplanetary magnetic field (IMF) is ~~directed~~ northward (IMF

$B_Z > 0$  nT) (e.g. Osmane et al. (2015)), magnetic reconnection on the dayside magnetopause is responsible for the majority of plasma transport across the magnetopause during southward interplanetary magnetic field IMF (IMF  $B_Z < 0$  nT), ~~which is also when allowing~~ the solar wind ~~couples to to drive activity in~~ the Earth's space environment ~~more efficiently~~ (Nishida, 1968; Koustov et al., 2009). The intervals of extended periods of strongly southward IMF typically arise when the Earth ~~is hit by encounters~~ an interplanetary coronal mass ejection (ICME) (see e.g. Kilpua et al. (2017b)). ICMEs are interplanetary counterparts of coronal mass ejections (CMEs), ~~gigantic large~~ eruptions of plasma and magnetic field from the Sun, ~~and it is now firmly established that ICMEs also drive~~ driving the strongest geomagnetic disturbances (e.g., Gosling et al. (1991); Huttunen et al. (2002); Richardson and Cane (2012); Kilpua et al. (2017a)). The signatures of ICMEs at 1 AU ~~have been debated since their first observational evidence: High include high~~ helium abundance (Hirshberg et al., 1972), high magnetic field magnitude and low plasma beta (Hirshberg and Colburn, 1969; Burlaga et al., 1981), low ion temperatures (Gosling et al., 1973), and smooth rotation of the magnetic field ~~Burlaga et al. (1981)~~ (Burlaga et al., 1981). While there have been attempts to form a universal set of signatures to describe ICMEs (Gosling, 1990; Richardson and Cane, 2003), they vary significantly such that no single set of criteria are able to describe all the ICME events, and none of them are unique to ICMEs. For example, only one third to one half of all the ICMEs have a magnetic flux rope (or a magnetic cloud) (e.g. Gosling, 1990; Richardson and Cane, 2003), whose signatures combine enhanced magnetic field, reduced proton temperature, and the smooth rotation of the magnetic field over an interval of a day (Burlaga et al., 1981). While magnetic clouds are the most studied part of ICMEs due to their significant potential to cause large space ~~weather~~ storms, their relationship to the entire ICME sequence still pose many questions (e.g., Kilpua et al. (2013)). Moreover, if the ICME is sufficiently faster than the ~~surrounding ambient~~ solar wind plasma, a shock is formed ahead of the ICME (Goldstein et al., 1998), with a region of compressed solar wind plasma between the leading shock front and the magnetic cloud, ~~that is~~ referred to as the sheath region. The ~~two regions~~, sheath and ejecta, ~~are~~ the most distinctive parts of ICMEs (see e.g. Kilpua et al. (2017b)), ~~which and~~ both can drive intense magnetic storms (e.g. Tsurutani et al. (1988); Huttunen and Koskinen (2004)). ~~Sheaths and ejecta, however, However, they~~ have clear differences in their solar wind conditions and consequently ~~differences in the solar wind-magnetosphere coupling (Jianpeng et al., 2010; Pulkkinen et al., 2007; Kilpua et al., 2017b). The reasons behind this different response is currently not fully understood, their coupling to the magnetosphere is different (Jianpeng et al., 2010; Pulkkinen et al., 2007; Kilpua et al., 2017b).~~ ICME sheaths typically include high solar wind dynamic pressure and fluctuating IMF ~~direction, with, including~~ both northward and southward orientations ~~occurring~~ within a short time period (Kilpua et al., 2017b). The duration of the sheath is also typically shorter than the following cloud, for example ~~in their study~~ Zhang et al. (2012) obtained the average values of 10.6 and 30.6 hours for sheaths and clouds, respectively. Sheaths are known to enhance high-latitude ionospheric currents (Huttunen and Koskinen, 2004), and they are found to have higher coupling efficiency than clouds (Yermolaev et al., 2012). The clouds typically enhance the equatorial ring current (Huttunen and Koskinen, 2004). Due to potential for strongly southward IMF orientation, ICME magnetic clouds ~~provide periods of the drive~~ enhanced magnetospheric activity. Moreover, during cloud events, due to the combination of generally high magnetic fields and low plasma densities, the solar wind Alfvén Mach number  $M_A$  can reach quite low values and even be close to unity. The role of  $M_A$  for solar wind - magnetosphere coupling has been highlighted in recent studies (Lavraud and Borovsky, 2008; Lopez et al., 2010;

Myllys et al., 2016, 2017). In particular, the role low  $M_A$  conditions typical to ICME magnetic cloud for the saturation of the ionospheric cross-polar cap potential CPCP has been a subject of several studies (e.g. Ridley, 2005, 2007; Lopez et al., 2010; Wilder et al., 2015; Myllys et al., 2016; Lakka et al., 2018).

Global MHD models have been ~~extensively~~ used to study the effects of ICMEs on the magnetospheric and ionospheric dy-

5 namics. Wu et al. (2015) used the H3DMHD model (e.g. Wu et al., 2007) to examine a CME event on March 15, 2013. They found that the high-energy solar energetic proton time-intensity profile can be explained by the interaction of a CME-driven shock with the heliospheric current sheet embedded within nonuniform solar wind. A recent paper by Kubota et al. (2017) studied the Bastille Day geomagnetic storm event (July 15, 2000) driven by a halo CME ~~that erupted from the Sun on July 14.~~ They found that the inclusion of auroral conductivity in the ionospheric part of the global MHD model by Tanaka (1994) led to ~~the saturated~~ saturation of the CPCP without any effect on the field-aligned currents, thus suggesting a current system with a dynamo in the magnetosphere and a load in the ionosphere. The difficulty in assessing these studies is that they often do not include uncertainty estimate of the model results, while the methods are different for each study. Moreover, while the different MHD simulations are based on the same plasma theory, the approaches are different in terms of exact form of the equations, the numerical solutions, and the initial and boundary conditions, thus making comparisons of different models difficult. Nonetheless, understanding of the performance limits of the simulations is essential for meaningful comparisons to in-situ measurements.

Regardless of the different approaches used in global codes, the performance of the models have been assessed in several studies. Usually such assessments have been done through comparisons of the simulation results with in situ or remote observations of dynamic events or plasma processes (Birn et al., 2001; Pulkkinen et al., 2011; Honkonen et al., 2013). This is often not easy, as even small errors in the simulation configuration may create large differences with respect to the observations locally at a single point (Lakka et al., 2017), even if the simulation would reproduce the large-scale dynamic sequence correctly. Moreover, recent studies (Juusola et al., 2014; Gordeev et al., 2015) have shown that none of the codes emerges as clearly superior to the others, each having their strengths and weaknesses. In the absence of uniform code performance testing methodology, validating the results individually is important.

25 In this study we use the GUMICS-4 (Janhunen et al., 2012), ~~the~~ global MHD simulation, and consider two ICME events, one ~~being significantly stronger in terms of the~~ having a significantly stronger solar wind driver than the other. To compare the two events, we use variables that are particularly sensitive to upstream changes, and examine how those variables are affected by the two events. The comparisons include the subsolar magnetopause position, the amount of energy transferred from the solar wind into the magnetosphere, the CPCP, and the magnetic field magnitude within the inner part of the magnetosphere. ~~We pay special attention to,~~ thus including both global and local variables. We especially focus on periods within the magnetic clouds within the ICMEs, by using two different spatial resolutions. We provide an uncertainty estimate (relative difference magnitude and standard deviation) for each quantity by comparing simulation results to well-established references, which include the Shue model (magnetopause location), the epsilon parameter (energy transferred through the magnetopause), the PCI index (CPCP), and in-situ measurements by Geotail and Cluster spacecraft (magnetic field magnitude).

This paper is structured in a following way: Section 2 describes GUMICS-4 global MHD code ~~and the simulation setup~~, Section ?? describes characteristics of the two ICME events ~~and the executed simulations~~, Section 4 presents the main results ~~from global and local perspectives, followed by discussion and~~ and Section ?? includes the discussion followed by conclusions.

## 5 2 Methodology

### 2.1 GUMICS-4 Global MHD Simulation

The simulations ~~in this study~~ were executed using the fourth edition of the Grand-Unified Magnetosphere-Ionosphere Coupling Simulation (GUMICS-4), in which a 3D MHD magnetosphere is coupled with a spherical electrostatic ionosphere (Janhunen et al., 2012). The finite volume MHD solver solves the ideal MHD equations with the separation of the magnetic field to a  
10 curl-free (dipole) component and divergent-free component created by currents external to the Earth ( $\mathbf{B} = \mathbf{B}_0 + \mathbf{B}_1(t)$ ) (Tanaka, 1994). The MHD simulation box has dimensions of 32 ... -224  $R_E$  in  $X_{GSE}$  direction and -64 ... +64  $R_E$  in both  $Y_{GSE}$  and  $Z_{GSE}$  directions, while the inner boundary is spherical with a radius of 3.7  $R_E$ . ~~In order to make the computations feasible on a single processor~~, GUMICS-4 uses temporal subcycling and adaptive cartesian octogrid. ~~The former to improve temporal and spatial resolution in key regions, which means that it only runs on a single processor due to difficulties in~~  
15 parallelizing computations with two adaptive grids. The temporal subcycling reduces the number of MHD computations an order of magnitude while maintaining the local Courant-Friedrichs-Levy (CFL) constraint (J.L. Lions, 2000, p. 121 — 151). The ~~latter~~ adaptive grid ensures that whenever there are large gradients, the grid is refined thus resolving smaller-scale features especially close to boundaries and current sheets.

The ionospheric grid is triangular and densest in the auroral oval, while in the polar caps the grid is still rather dense, with  
20 about 180 km and 360 km spacing used in the two regions, respectively. The ionosphere is driven by field-aligned currents ~~and electron precipitation from the magnetosphere~~, as well as by solar EUV ionisation. Field-aligned currents contribute to the cross-polar cap potential through

$$\nabla \cdot \mathbf{J} = \nabla \cdot [\Sigma \cdot (-\nabla \phi + V_n \times \mathbf{B})] = -j_{||} (\hat{\mathbf{b}} \cdot \hat{\mathbf{r}}), \quad (1)$$

where  $\mathbf{J}$  is current density,  $\Sigma$  is the height-integrated conductivity tensor,  $\phi$  is the ionospheric potential,  $V_n$  the neutral wind  
25 caused by the Earth's rotation,  $j_{||}$  is the field-aligned current, and  $(\hat{\mathbf{b}} \cdot \hat{\mathbf{r}})$  is the cosine of the angle between the magnetic field direction  $\hat{\mathbf{b}}$  and the radial direction  $\hat{\mathbf{r}}$  (Janhunen et al., 2012). Electron precipitation and solar EUV ionisation have contributions on the height-integrated Pedersen and Hall conductivities with solar EUV ionisation parametrized by the 10.7 cm solar radio flux that has a numerical value of  $100 \times 10^{-22} \text{ W/m}^2$ . Electron precipitation affects the altitude-resolved ionospheric electron densities, ~~which are calculated at different altitudes~~ and are used when computing the height-integrated Pedersen and Hall con-  
30 ductivities. The details on the ionospheric part of GUMICS-4 can be found in ~~Janhunen and Huuskonen (1993)~~ Janhunen and Huuskonen (1993).

The region between the MHD magnetosphere and the electrostatic spherical ionosphere is a passive medium where no currents flow perpendicular to the magnetic field. The magnetosphere is coupled to the ionosphere using dipole mapping of the field-

aligned current pattern and the electron precipitation from the magnetosphere to the ionosphere and the electric potential from the ionosphere to the magnetosphere. This feedback loop is updated every 4 seconds.

## 2.2 GUMICS simulations of two ICME events

- We use both 0.5 and 0.25  $R_E$  maximum spatial resolutions as well as varying dipole tilt angle in this study. Two complete ICME periods were simulated using 0.5  $R_E$  resolution by starting with nominal solar wind conditions preceding the events, and ending with nominal conditions following the events. To give GUMICS-4 magnetosphere time to form [Lakka et al. \(2017\)](#) ([Lakka et al., 2017](#)), the simulations were initialized with two hours of constant solar wind driving using upstream values equal to those ~~used~~ during the first minute of the actual simulation ( $n, |V|, |B|$  values of  $4 \text{ cm}^{-3}$ ,  $310 \text{ km/s}$  and  $1.1 \text{ nT}$  for the 2012 event, and  $11 \text{ cm}^{-3}$ ,  $300 \text{ km/s}$  and  $1.8 \text{ nT}$  for the 2014 event).
- Due to computational limitations, using the best maximum spatial resolution (0.25  $R_E$ ) covering both ICME events with full length is not feasible. ~~Hence~~ due to long simulation physical time (up to 3.5 days) and resulting long simulation running times. Hence, two additional runs were performed with 0.25  $R_E$  maximum spatial resolution in order to gain a more detailed view of the dynamics of the magnetosphere and ionosphere when the ICME magnetic cloud was propagating past the Earth. These runs lasted 6 hours each, and were executed by restarting the 0.5  $R_E$  runs with enhanced resolution. Table 1 summarizes all four simulation runs related to the study.

## 3 Observations of two ICME events

- We ~~retrieve~~ use the solar wind data from the NASA OMNIWeb service (<http://omniweb.gsfc.nasa.gov>) and the solar energetic particle data from the NOAA NCEI Space Weather data access (<https://www.ngdc.noaa.gov/stp/satellite/goes/index.html>) ~~for the two ICME events studied here~~. Onset times for the ICME sheath (i.e., the shock time) and the magnetic cloud boundary times are retrieved from the Wind spacecraft ICME catalogue (<https://wind.nasa.gov/ICMEindex.php>). Figures 1 and 2 show the upstream parameters during both events. For both figures, IMF  $X, Y, Z$  components and the IMF magnitude are shown in panel a, upstream plasma flow velocity  $X, Y, Z$  components in panel b, the upstream plasma number density in panel c, upstream Alfvén Mach number (in logarithmic scale) in panel d, energetic proton fluxes for three GOES-15 energy channels between 8–80 MeV in panel e, and the cross-polar cap potential from the GUMICS-4 simulation in panel f. Figure 1 includes time range from 09:00 UT, July 14 to 15:00 UT, July 17, 2012, while Figure 2 shows the period from 19:00 UT, April 28 to 17:00 UT, May 1, 2014. The time of the ICME shock, and the start and end times of the ICME are marked with vertical red lines in both figures. The ~~gray-shaded~~ grey-shaded regions indicate the time periods simulated with the maximal 0.25  $R_E$  spatial resolution. Both IMF and plasma flow velocity components are given in GSE coordinate system, which is also the coordinate system used by the GUMICS-4 simulation.
- Figure 1 shows the arrival of the leading shock at 18:53 UT on July 14, 2012 as the simultaneous abrupt jump in the plasma and magnetic field parameters and the following ICME sheath as irregular directional changes of the IMF and compressed plasma and field. The energetic particle fluxes for the two lower energy channels increase until after the shock passage, which suggests

continual particle acceleration in the shock driven by the ICME. At 06:54 UT on July 15, the onset of the ICME magnetic cloud is identified by ~~the strong southward~~ turning of the IMF ~~orientation to strongly southward~~, Significant reduction in the number density~~reducing significantly~~, and the clear decrease in the variability of the interplanetary magnetic field. During the next 45 hours, the IMF direction ~~stays strongly southward and it rotates slowly~~ stayed strongly southward while slowly rotating towards less southward orientation. We note that in the trailing part of the ICME, the field changes rather sharply to northward ~~orientation and there continues to rotated to south~~, thereafter continuing to rotate southward again. We cannot rule out that this end part is not another small ICME, but as our study focuses on the strong southward magnetic fields in the main part of the ICME we do not consider the origin of this end part further here.

The ICME on April 2014 was slower than the July 2012 ICME and its speed ~~is was~~ very close to the ambient solar wind speed. Hence, no shock, nor clear sheath developed ahead of this ICME. The onset of the ~~ICME-related~~ ICME-related disturbance is marked by the increased plasma number density followed by a rapid decrease and a clear southward turning of the IMF at 20.38 UT on April 29 (Figure 2). The ~~lack of shock is also supported~~ weaker activity is also evident by the lack of energetic particle fluxes above background in the magnetosphere. The very ~~beginning~~ early phase of this cloud may contain some disturbed ~~preceding~~ solar wind (the region of higher density and fluctuating field), but we do not ~~separate it in this study~~ identify it as a sheath and focus our study on the effects of the cloud ~~part~~ proper.

Both magnetic clouds are ~~featured with~~ characterized by low Alfvén Mach number. In the 2012 case,  $M_A$  ~~falls~~ drops even below unity and is 1.9 on average during the cloud structure, while during the 2014 magnetic cloud, the minimum  $M_A$  was 3.8 and ~~the average was 5.8~~ on average.

The 2012 event features generally larger CPCP, with ~~its values residing~~ values above 40 kV, ~~increasing gradually~~ and reaching 70 kV (Figure 1f). ~~Opposite to this~~, On the other hand, during the 2014 event the CPCP peaks early ~~to reach at~~ 50 kV during the 2014 event and subsequently reduces to 20 kV (Figure 2f).

The 2012 ICME event is considerably longer than the 2014 event, with ~~57 hours 26 minutes~~ 57h 26min total duration, of which ~~12 hours 1 minute~~ 12h 1min are sheath, and ~~45 hours 25 minutes belong to~~ 45h 25min part of the magnetic cloud passage. The 2014 event lasted 21 ~~hours~~ h 13 ~~minutes~~ min in total. The 2012 ICME had larger effects on magnetospheric dynamics activity, as the solar wind driving was considerably stronger, with the average IMF magnitude and solar wind speed of 14 nT and 490 km/s, respectively, compared with 8.5 nT and 303 km/s of the 2014 event. The maximum IMF magnitude and upstream solar wind speed were also larger during the 2012 event, with 21 (10) nT and 660 (321) km/s maximum values measured during the 2012 (2014) cloud. However, while maximum number density was higher during the 2012 magnetic cloud ( $36 \text{ cm}^{-3}$  vs.  $30 \text{ cm}^{-3}$ ), the average number density was considerably higher during the 2014 event (2012:  $2 \text{ cm}^{-3}$  vs. 2014:  $12 \text{ cm}^{-3}$ ).

During the two ICME events, data from the Cluster 1 (hereafter Cluster) and Geotail satellites were available from the CDAWeb service (<https://cdaweb.sci.gsfc.nasa.gov/index.html>). Figure 3 shows the orbits of Cluster (blue) and Geotail (~~magenta~~ green) along with the magnetopause location (black) from the empirical Shue model ~~Shue et al. (1997)~~ (Shue et al., 1997) on the  $XY$  plane (figures 3a and 3c) and on the  $XZ$  plane (figures 3b and 3d) during for both events. ~~Magnetopause~~ The magnetopause position is computed for the most earthward magnetopause location during the events. ~~Note that~~, while the orbit tracks include intervals of nominal upstream conditions before and after the ICME events. ~~Starting points and ending~~ Start and end points of

35 the time intervals ~~under inspections~~ are marked with a cross and a triangle, respectively. Dots mark the ~~(located visually)~~ points where satellite orbits intersect ~~(located visually) the innermost position of~~ the magnetopause. ~~It should be noted that since~~ ~~The variability of~~ the magnetopause position ~~is not stable, but rather in motion during the events, the intersection points are only approximations~~ means that ~~between those orbit tracks the S/C may cross to outside the magnetosphere~~. The used coordinate system is GSE. Based on figure 3, the Cluster spacecraft orbits inside of the magnetosphere throughout the 2012 event and  
5 ~~for~~ most of the 2014 event. On the other hand, Geotail is outside ~~of~~ the magnetosphere an extended period during July 16-17, ~~2012-2012~~ as well as during ~~April 28, late April 30, and early May 1 in several periods in April-May~~ 2014.

Figures 4 and 5 show time series of the magnetic field magnitude  $|B|$  along the Geotail (panel a) and Cluster (panel b) orbits during the 2012 and 2014 events. ~~Magenta-Green~~ (Geotail) and blue (Cluster) curves show the ~~actual in-situ data~~ observations, while the black ~~(magenta)~~ curve shows the magnetic field magnitude along the spacecraft orbits in GUMICS-4 simulation ~~;~~  
10 ~~The gray-shaded using 0.5 (0.25)  $R_E$  maximum spatial resolution. The yellow-shaded~~ regions in panels a and b ~~show when the respective spacecraft is outside the magnetosphere according to Figure 3 indicate times when the spacecraft may encounter magnetopause crossings~~. Note that a logarithmic scale is used for the Cluster data. Panel c in both figures shows the radial distance of ~~both the~~ spacecraft from the center of the Earth. ~~Note that satellite measurements have been interpolated over long (several hours) datagaps, most notably on July 16, 12:15–18:45 UT.~~

15 At the start of the 2012 event, Geotail resides in the plasma sheet, but quickly moves to the boundary layer (roughly July 14, 16:00 UT to July 15, 06:00 UT), after which it enters the lobe as the cloud proper hits the magnetosphere. At around the ~~time of the~~ end of the data gap ~~towards at~~ the end of July 16, the spacecraft moves to the low latitude boundary layer and the magnetosheath (~~supported by the identified from~~ plasma data not shown here).

At the start of the 2012 event, Cluster is near perigee recording field values ~~close to those of the dipole dominated by the dipole~~  
20 ~~contribution~~. Cluster exits the ring current region around 16:00 UT on July 14, and enters the plasma sheet. A brief encounter in the lobe is recorded between roughly 18:00 UT July 15 and 06:00 July 16. A second period in the inner magnetosphere commences around 12:00 UT on July 16, with exit to the lobe after 00:00 UT July 17 (~~supported by the identified from~~ plasma and energetic particle data not shown here).

## 4 Analysis

### 25 4.1 Global dynamics

Figures 6 and 7 show the effect of upstream IMF  $B_Z$  (panel a), and solar wind dynamic pressure (panel b) on the magnetopause nose (panel c), total energy through the dayside magnetopause ~~nose position~~ (panel d) and the ionospheric cross-polar cap potential CPCP (panel e) during the ~~6-hour intervals run in higher resolution (gray shading simulated intervals shown~~ in figures 1 and 2. The  $0.5 R_E$  resolution run results are shown in black, and  $0.25 R_E$  resolution results are shown in magenta. ~~We Grey~~  
30 ~~shaded area highlights the 6-hour interval simulated using both resolutions. Blue and green curves indicate reference values (see below) and solar wind upstream conditions, respectively.~~

As a metrics for validating the simulation results, we use the magnitude of the relative difference (given as  $\delta$  in panels c, d and e of figures 6 and 7).

$$\delta = \left| \frac{x_{\text{ref}} - x_{\text{GUMICS-4}}}{x_{\text{ref}}} \right|, \quad (2)$$

in which  $x$  is the GUMICS-4 variable and  $x_{\text{ref}}$  refers to the reference parameter value of the variable. An average  $\delta$  value is computed for each ICME simulation phase (nominal solar wind, sheath, cloud) for both  $0.5 R_E$  and  $0.25 R_E$  resolution runs. These percentage values can be found in tables 2 and 3. We also compute standard deviation (SD) for the reference vs. GUMICS-4 results. A single SD value (given in panels c, d and e) is computed for the  $0.5 R_E$  resolution runs to illustrate how similar the temporal evolution is over time scales of days for GUMICS-4 and the reference parameter.

Figures 6a and 6b show that the IMF  $B_Z$  fluctuates approximately between  $-5..+5$  nT during nominal solar wind conditions, while the solar wind dynamic pressure is steady and low. At the onset of ICME sheath, both  $B_Z$  and dynamic pressure start fluctuating with increased amplitude. Moreover, after the onset of ICME cloud, the orientation of the IMF slowly rotates from southward to northward with the solar wind dynamic pressure decreasing rapidly and remaining low until the end of the simulated interval. This behaviour is somewhat similar during the 2014 event (figures 7a–7b), with the exception of missing high amplitude fluctuations due to absence of a distinct ICME sheath.

In GUMICS-4, we identify the magnetopause nose position from as a single grid point having the maximum value of  $J_Y$  along the Sun-Earth lineat, using one-minute temporal resolution, smoothed using 10-min sliding averages. This value is compared with the Shue (Shue et al., 1997) empirical magnetopause model. ~~Total energy through the dayside magnetopause is computed by evaluating the Poynting flux in the vicinity of the (Shue) magnetopause, and its component parallel to the magnetopause surface normal. These values are integrated over the surface of the~~ For simplicity, the nose of the magnetopause ~~Sunward of the terminator~~ is referred to a magnetopause. Figure 6c shows that at the onset of ICME sheath, the magnetopause moves Earthward as a consequence of changing upstream conditions, which is followed by Sunward return motion lasting until the end of the ICME event. The average  $\delta$  is highest during the cloud (8%) and lowest (2.5%) during nominal solar wind conditions. During ICME sheath, average  $\delta$  is 4.5%. During the 2014 event, the magnetopause starts moving Earthward at least 10 hours before the onset of ICME cloud (figure 7c), as the dynamic pressure increases, with IMF  $B_Z$  staying positive. After the onset however, the magnetopause moves Sunward for a few hours until slowly moving Earthward again. The difference in average  $\delta$  between cloud and nominal solar wind conditions is lower than for the 2012 event, as the respective values are 3.3% and 2.4%.

~~Figure~~ The grey-shaded region in figure 6c shows that during the first four hours of the 6-hour run the magnetopause position predictions (black and magenta curves) by GUMICS-4 are ~~close to~~ within 5% of the Shue et al. (1997) model (blue curve). During the last 2 hours, however, there are more fluctuations in the GUMICS-4 magnetopause position, especially in the  $0.5 R_E$  resolution run. From July 15, 21:00 UT to July 16, 01:00 UT the simulation runs agree on the magnetopause location and also with the Shue model, with differences within 10% all the time of the first 4 hours. However, the last two hours show more variations between the three curves: The finest resolution show slight outward motion of the magnetopause, which toward the end of the period is less than that predicted by the Shue model. On the other hand, the  $0.5 R_E$  resolution run shows inward indentations followed by outward motion consistent with the Shue model. Overall, the  $0.5 R_E$  resolution run is 58% of the time

within 10% of the Shue model, and the 0.25  $R_E$  resolution run agree 67% of the time within 10% of the Shue model. ~~Over the entire~~ Despite the fact that average relative difference is slightly lower for the 0.5  $R_E$  resolution run (4.9%) than for the 0.25  $R_E$  resolution run (5.6%), over the entire 6-hour periods, the 0.25  $R_E$  run is within 10% of the Shue model 92% of the time, while the 0.5  $R_E$  run reaches within 10% 89% of the time -

5 ~~After the increase of the IMF  $B_Z$  from -16 to -14 during the first hour, hours from 22 to 01 feature steady IMF  $B_Z$  and slightly fluctuating solar wind dynamic pressure (figures 6a-6b), while the last 2 hours due to the conditions change, with IMF  $B_Z$  increasing gradually and the dynamic pressure dropping below 0.5 . In these conditions,  $R_E$  run being more inclined toward moving more Earthward during the last two hours of the 6-hour period.~~

The time evolution of the magnetopause position during the 6-hour period in Figure 7 is similar for both spatial resolutions, with both simulation runs responding similarly to small upstream fluctuations. Both simulation runs stay within 10% of the Shue model ~~predicts the magnetopause nose to move sunward, as does GUMICS-4, albeit the accuracy of the predictions depends on the used resolution~~ prediction for the entire 6-hour period. Average relative difference is only slightly lower for the higher resolution run (3.2%), than for the lower resolution run (4.5%).

15 ~~The~~ Overall, the higher-resolution run yielded better agreement with the magnetopause location especially for a moving magnetopause nose (2012 event), because increasing the spatial resolution sharpens the gradients and allows better identification of the location of the maxima (Janhunen et al., 2012). Comparison of the runs shows, however, that the results are consistent with each other, indicating that the lower-resolution run is providing similar large-scale dynamics as the finer-resolution run. Furthermore, increased  $\delta$  during the 2012 ICME cloud and overall higher  $\delta$  during the 2012 event indicate that GUMICS-4 accuracy in the magnetopause nose position prediction is better during weaker solar wind driving. This is further demonstrated by the standard deviation values, which are 0.661 for the 2012 event, and 0.321 for the 2014 event (see figures 6c and 7c).

Total energy through the dayside magnetopause is computed by evaluating the energy flux incident at the (Shue) magnetopause, and it is evaluated from

$$\mathbf{K} = \left( u + p - \frac{B^2}{2\mu_0} \right) \mathbf{V} + \frac{1}{\mu_0} \mathbf{E} \times \mathbf{B}, \quad (3)$$

25 where  $u$  is the total energy density,  $p$  pressure,  $B$  magnetic field,  $\mathbf{V}$  flow velocity and  $\mathbf{E} \times \mathbf{B}$  the Poynting flux, and its component perpendicular to the magnetopause surface. As is shown in figure 6c, the relative difference magnitude  $\delta$  in the magnetopause nose location can reach up to 30% values. To avoid underestimating the size of the magnetosphere, we evaluate the magnetopause surface by moving the radial distance of each Shue magnetopause surface value 30% further away from the Earth. This surface is then used in integrating the energy flux values entering the magnetosphere Sunward of the terminator ( $X > 0 R_E$ ). The results are shown for the 2012 event in figure 6d for both 0.5 and 0.25  $R_E$  resolution runs along with the computed  $\epsilon$ -parameter (Perreault and Akasofu, 1978):

$$\epsilon = \frac{4\pi}{\mu_0} V B^2 \sin^4\left(\frac{\theta}{2}\right) l_0^2, \quad (4)$$

where  $\mu_0$  is vacuum permeability,  $B$  and  $V$  are the magnitudes of the IMF and solar wind plasma flow velocity,  $\theta$  is the IMF clock angle, and  $l_0$  is an empirically determined scale length.

While both resolution runs agree with each other, it is evident that their numerical values are quite far from the reference,  $\epsilon$ -parameter. It should be noted however, that the  $\epsilon$ -parameter is not scaled to represent the energy input, but the energy dissipated in the inner magnetosphere (?). Thus the relative difference is not a good metrics to describe the difference between GUMICS-4 and the  $\epsilon$ -parameter. However, general temporal evolution is similar for most parts of ICME cloud, with both GUMICS-4 and the  $\epsilon$ -parameter reproducing steep increase at the onset of cloud as well as subsequent slow decrease, as is shown by the computed SD value in figure 6d (2.263). As in the case of the 2012 event, the two simulation runs using different spatial resolutions are almost inseparable in terms of the incoming solar wind energy during the 2014 event (Figure 7d). During moderate solar wind driving in 2014, GUMICS-4 is closer to the  $\epsilon$ -parameter, with considerably lower SD value (0.725) compared with the 2012 event. This is an interesting characteristics of the  $\epsilon$ -parameter warranting further study.

Differences between the simulations executed using different spatial resolutions in local measures, such as the magnetopause nose position, do not show in global variables, such as the total energy through the dayside magnetopause surface. As can be seen from in Figure 6d, the curves of the two different spatial resolution runs are almost identical. This emphasizes the interpretation—that integrated quantities, such as energy, which—give a better representation of the true physical properties of the magnetosphere in the GUMICS-4 solution, and are not dependent on grid resolution (Janhunen et al., 2012). We acknowledge that using more sophisticated methods for computing identifying the magnetopause surface from the simulation could potentially lead to more accurate some changes in the results. The Shue model was however used since it is relatively easy to apply and also because most of the large-scale variations with respect to the measurements occur in the nightside magnetopause, which is neglected in this study. In addition, our results are mostly of the same order of magnitude compared to what was obtained by Palmroth et al. (2003) used for its simplicity and computational ease. Our results agree in general with Palmroth et al. (2003) who identified the magnetopause by using plasma flow streamlines for computing the magnetopause surface from GUMICS-4 results, indicating that the use of the Shue model is not introducing large errors in the energy estimates. The magnetosphere – ionosphere coupling, however, here illustrated by the CPCP time evolution in Figure 6 demonstrates differences between the, is compared with the polar cap index (Ridley and Kihn, 2004) computed as

$$PCI = 29.28 - 3.31\sin(T + 1.49) + 17.81PCN, \quad (5)$$

where  $T$  is month of the year normalized to  $2\pi$ , and  $PCN$  is the northern polar cap index retrieved from OMNIWeb. The PCI is a very indirect proxy (based on a single-point measurement only) for the CPCP, and thus the comparisons must be interpreted with great care. It is worth noting, that for the 2012 event, GUMICS-4 is closest to PCI in terms of  $\delta$  during the ICME cloud, with 36.0% average difference between the two. The difference is larger during nominal solar wind conditions and ICME sheath phase, with average  $\delta$  values of 64.9% and 57.6%.

The 0.25  $R_E$  and the 0.5  $R_E$  runs, with differ from each other in terms of the polar cap potentials. For the 2012 event, the higher resolution run producing produces 20-30% higher CPCP than the lower resolution run during the first three hours after the 0.25 run has stabilized, which happens within 10 minutes after July 15, 21:00 UT of the 6-hour phase. During the last 3 hours, the

CPCP predicted by the  $0.5 R_E$  run increases significantly to almost reach the high-resolution run cross-polar cap potential. This coincides with the time when the magnetopause ~~has moved~~ moves further away from the Earth ~~in the simulations~~. ~~The expansion of the magnetosphere is also verified by the Shue model.~~

~~The time evolution of the magnetopause position in Figure 7 is similar regardless of the used spatial resolution, with both simulation runs responding similarly to small upstream fluctuations. Both simulation runs stay within 10% of the Shue model prediction for the entire 6-hour period. As in the case of the 2012 event, the two simulation runs are almost inseparable in terms of the incoming solar wind energy (Figure 7d) period simulated using both resolutions.~~

Figure 7e shows that the relative difference between the PCI index and GUMICS-4 is greatest during ICME cloud (69.2% on average) compared with 46.9% average difference during nominal solar wind conditions. However, while the 2012 and 2014 events are similar ~~also~~ in terms of higher CPCP in the fine resolution simulation (up to 250% in the 2014 event), CPCP is quite stable ~~in~~ during the 2014 event in both low and high resolution throughout the 6 hour interval. As in the case of the 2012 event, the higher resolution run is closer to the PCI index, with average relative difference resulting as 70.0% and 27.0% for the  $0.5$  and  $0.25 R_E$  resolution runs respectively during the 6-hour phase.

In terms of the SD values, GUMICS-4 and the PCI index show better agreement in the temporal evolution of CPCP during the 2014 event ( $SD = 15.838$ ) than during the 2012 event ( $SD = 5.107$ ). However, these SD values are clearly highest of all three (magnetopause nose, energy, CPCP) for both events. This is in part due to the ionospheric (local) processes contributing to the PCI index but not related to the large-scale potential evolution.

## 4.2 Saturation of the Cross-polar cap Potential

Figures 8 and 9 show the CPCP (both northern and southern hemispheres ~~are considered~~) as a function of the solar wind electric field  $E_Y$  component for both ICME events. Color-coding marks the IMF magnitude in figures 8a and 9a, solar wind speed in figures 8b and 9b, and the upstream Alfvén Mach number in figures 8c and 9c. Every data point in Figure 8 (9) is computed from 10-minute averages, binned by  $E_Y$  with 1.0 (0.5) mV/m intervals. The ICME sheath (solid circles) and cloud (solid squares) periods as well as the nominal solar wind conditions (solid triangles) prior to and following the events are analyzed separately. Note that here only the coarse grid ( $0.5 R_E$ ) simulation results are used, as we analyze the effects during the entire magnetic cloud and sheath periods including times before and after the event not covered by the high-resolution run.

Figure 8 shows that the response of the CPCP to the upstream  $E_Y$  is quite linear during the magnetic cloud (squares) when solar wind driving electric field  $E_Y$  is below 5 mV/m, during nominal solar wind conditions (triangles), and ICME sheath (~~tilted squares~~ diamonds). However, the polar cap potential first decreases and subsequently saturates during the cloud when the solar wind driving is stronger ( $E_Y > 5$  mV/m). For the 2012 event, we refer to the  $E_Y$  range from 0 to 5 mV/m as the linear regime, and from 5 mV/m upward as the non-linear regime.

Figure 8a shows the obvious result that highest  $E_Y$  values are associated with highest IMF magnitudes. However, it also shows that the largest IMF magnitudes are associated with the non-linear regime, indicating that strong upstream driving leads to ~~the~~ CPCP saturation. In addition, Figure 8b suggests that the increase of the CPCP in the linear regime is clearly higher for

lower velocity values (cloud structure), than for higher velocity values (sheath and nominal conditions). Generally, this agrees with the previous studies utilizing statistical (Newell et al., 2008) and numerical (Lopez et al., 2010) tools. The latter authors suggest that this is caused by the solar wind flow diversion in the pressure gradient-dominated magnetosheath; faster solar wind will produce more rapid diversion of the flow around the magnetosphere, and thus smaller amount of plasma will reach the magnetic reconnection site.

Figure 8c shows that the upstream Alfvén Mach number  $M_A$  is at or above 4 ( $M_A \geq 4$ ) during the nominal solar wind conditions and during the ICME sheath, while during the magnetic cloud  $M_A$  resided below 4 and almost reaches unity. This supports the interpretation that saturation of the CPCP depends on the upstream Alfvén Mach number  $M_A$  such that saturation occurs only when  $M_A$  values fall below 4. The dependence of the CPCP saturation on  $M_A$  is well-known, documented both in measurements (Wilder et al., 2011; Myllys et al., 2016) and in simulation studies (Lopez et al., 2010; Lakka et al., 2018).

Figure 9 ~~seems to agree~~ agrees with the view presented above, as the response of the CPCP to the upstream  $E_Y$  during the 2014 event is quite linear regardless of the IMF magnitude (Figure 9a), plasma flow speed (Figure 9b), or the large-scale solar wind driving structure (ICME cloud or nominal solar wind), ~~which however do not vary very much during the event~~. This is apparently because solar wind driving is substantially weaker during the 2014 event than during the 2012 event, with the IMF magnitude reaching barely 10 nT, and upstream plasma flow speed varying only of the order of 10 km/s. As a result, the upstream Alfvén Mach number  $M_A > 4$  throughout the ICME event as well as during the nominal solar wind conditions. The high polar cap potential values for the lowest  $E_Y$  bin is associated with the large density enhancement driving polar cap potential increase before the arrival of the cloud proper.

Figure 10 shows the region 1 and region 2 field-aligned current (FAC) system ~~as an indicator of the coupling of coupling~~ the magnetosphere and the ionosphere (e.g. Siscoe et al. (1991)). The four panels show how field-aligned currents are distributed in the northern hemisphere ionosphere in July 16, 2012 at 01:00 UT and 03:00 UT at 0.5  $R_E$  maximum resolution (figures 10a–10b) and at 0.25  $R_E$  maximum resolution (figures 10c–10d). Current density is shown both as color coding and contours, while the white dotted line depicts the polar cap boundary. The distribution of the FAC do not change much in either of the simulations, thus suggesting that the coupling of the magnetosphere and the ionosphere remains relatively constant. However, as is shown in figure 6e, the CPCP shows different temporal evolution based on the used spatial resolution, with increasing (constant) CPCP in the 0.5 (0.25)  $R_E$  simulation, thus suggesting that while the magnetosphere - ionosphere coupling is unaffected, the solar wind - ionosphere coupling is affected of enhanced spatial resolution.

### 30 4.3 Local dynamics

Figures 4 and 5 show the time series of the IMF magnitude  $|B|$  in the Geotail and Cluster orbits during the 2012 and 2014 events compared with the GUMICS-4 results along the satellite tracks. ~~Overall, GUMICS-4 underestimates~~ The relative difference magnitude in  $|B|$  measured by both satellites, but the time evolution of the magnetic field is generally similar between GUMICS-4 and both satellites as well as standard deviations are computed using the same methods as in section 4.1, and are given in panels a and b. Since the inner boundary of the GUMICS-4 MHD region is at 3.7  $R_E$ , the times when Cluster is closer than 3.7  $R_E$  to Earth are ignored when computing  $\delta$  and SD values.

Prior to the arrival of the sheath region in ~~the 2012 event~~, Geotail enters the plasma sheet boundary layer earlier than predicted by GUMICS-4. During the ICME sheath there are many dips and peaks in both plots, with the difference between measured (both Geotail and Cluster) and predicted values varying, as can be seen from figures 4a and 4b. Also, Figure 4a shows that starting from July 17, 0006:00 UT the in-situ value in Geotail orbit measured field at Geotail increases as the satellite goes to the magnetosheath proper, while GUMICS-4 prediction decreases as the orbit track in GUMICS-4 approaches the shock region (see Figure 3a). The 2014 event shows similar features especially when Geotail enters and exits the magnetosphere at 23:14 UT, April 28, and at 12:00 UT, April 30, respectively, with measured (by Geotail)  $|B|$  in the former case fluctuating and rising sharply from 10 nT to 40 nT while the predicted GUMICS-4  $|B|$  increases more steadily from a few nT to 20 nT as the satellite enters from the magnetosheath to the magnetosphere. In the latter case decrease (increase) of measured (simulated)  $|B|$  occurs several hours after the spacecraft exits the magnetosphere (later grey-shaded yellow-shaded region in Figure 5a) possibly because of the inaccuracies in defining differences in the moment of exit (and exact location of the magnetopause location). Note that while Cluster makes an entry into the magnetosphere at 16:12 UT, April 29, GUMICS-4 predicts a position within the magnetosheath and an entry into the magnetosphere only following the end of the cloud. Note that the Cluster perigee ( $2 R_E$ ) (Figure 4c) is below the inner boundary of the GUMICS-4 simulation ( $3.7 R_E$ ), which causes the simulation field to record unphysical values around the time of the maximas maxima at 09:00 on July 14, 2012 and 15:00 on July 16, 2012, and hence there are hence the data gaps in GUMICS-4 data plots.

The effect of the ICME sheath is visible after the onset of the sheath its arrival in Figure 4, with both measured and predicted  $|B|$  fluctuating. The ICME magnetic cloud proper seems to cause largest difference in  $|B|$  during the 2012 event, when the driving was quite strong.

Tables 4 and 5 summarize average  $\delta$  over each ICME phase (nominal solar wind conditions, sheath, cloud). Moreover, average  $\delta$  is given also over times when the spacecraft is located inside and outside the magnetosphere. The relative difference magnitude in  $|B|$  between GUMICS-4 and in-situ measurements ranges between 34.4% and 79.7%, depending on ICME phase, with GUMICS-4 values being mostly larger than those measured by either of the two spacecraft. Overall,  $\delta$  is lower between GUMICS-4 and Cluster than between GUMICS-4 and Geotail. Largest  $\delta$  between GUMICS-4 and Cluster in 2012 is created during the ICME sheath (59.2%), however, this phase creates lowest  $\delta$  when comparing GUMICS-4 and Geotail (41.9%). The difference in  $\delta$  between nominal solar wind conditions and ICME cloud phase is considerably lower for the 2012 event (61.4% and 66.6%) than for the 2014 event (55% and 79.7%) when comparing GUMICS-4 and Geotail. Similar trend is observable if comparison between GUMICS-4 and Cluster is considered (37.3% and 52.7% for the 2012 event, 36.5% and 62.9% for the 2014 event), albeit with slightly lower magnitude. Moreover, while  $\delta$  is quite similar regardless of Geotail position with respect to the magnetopause in both 2012 and 2014, it increases from 34.4% to 60.8% during the 2014 event between GUMICS-4 and Cluster. The standard deviations (SD) over the simulated time ranges using  $0.5 R_E$  spatial resolutions are considerably lower on Geotail orbit (2012: 5.476, 2014: 6.564) than on Cluster orbit (2012: 25.054, 2014: 24.795).

## 5 Discussion

In this paper we study [1](#)) how the magnetosphere responds to two ICME events with different characteristics by means of using the GUMICS-4 global MHD simulation, [and 2](#)) [how accurately GUMICS-4 reproduces the effects of the two events](#). The 2012 event was stronger in terms of solar wind driver, the 2014 event being significantly weaker both in terms of solar wind speed and IMF magnitude. We considered both global and local parameters, including magnetopause nose position along the Sun-Earth [-heliosphere](#), total energy transferred from the solar wind into the magnetosphere, and the ionospheric cross-polar cap potential (CPCP). Local measures include response of the magnetic field magnitude along the orbits of Cluster and Geotail spacecraft. The two ICME events were simulated using  $0.5 R_E$  maximum spatial resolution. To test the effect of grid resolution enhancement on global dynamics, we simulated ~~6-hour~~ [6-hour](#) subsets of both CME cloud periods with  $0.25 R_E$  maximum spatial resolution. [As an uncertainty metrics we use both relative difference magnitude  \$\delta\$  and standard deviation SD.](#)

[Due to stronger solar wind driving, the 2012 event causes the magnetosphere to compress more than during the 2014 event, with the magnetopause moving Earthward at the onset of the 2012 ICME sheath and reaching  \$7 R\_E\$  distance from Earth, until moving Sunward at the onset of ICME magnetic cloud \(see figure 6c\). Both ICMEs are preceded by low IMF  \$B\_z\$  and solar wind dynamic pressure, with the 2014 missing high amplitude fluctuations before ICME cloud due to absence of separate ICME sheath. Despite this, the movement of the magnetopause is similarly Earthward prior to the cloud, reaching  \$9.5 R\_E\$  just before the onset of the cloud \(see figure 7c\). During the cloud however, the orientation of the IMF slowly rotates from southward to northward and the magnetopause is in constant Sunward \(Earthward\) motion in 2012 \(2014\). While the polarity of the IMF changes before the end of the ICME in 2012, it changes from southward to northward only after the end of the ICME in 2014.](#)

The magnetopause ~~location changes~~ [nose location in GUMICS-4 is identified as a single grid point from the maximum value of  \$J\_y\$  along the Sun-Earth line. Location deviations](#) in response to solar wind driving in the GUMICS-4 results is dependent on the driver intensity: Stronger driving during the 2012 CME magnetic cloud leads to larger ~~differences~~ [relative difference magnitude  \$\delta\$  \(2012:  \$8.0\% \delta\$  on average\)](#) as compared to the ~~(Shue et al., 1997)~~ [Shue et al. \(1997\)](#) model, whereas the agreement between the simulation and the empirical model is quite good [\(3.3%  \$\delta\$  on average\)](#) during weaker driving during the 2014 event (figures 6 and 7). [This view is further supported by standard deviations \(SD\): For the full simulation time range SD is 0.661 \(0.321\) in 2012 \(2014\). Average  \$\delta\$  during nominal solar wind conditions is almost identical for both events: 2.5% for the 2012 event and 2.4% for the 2014 event.](#)

Comparison of the magnetopause location between the  $0.25 R_E$  ( $0.5 R_E$ ) resolution run and the Shue model show that the relative difference between the two is below 10% 92% (89%) of the 6 hour subset in 2012 (Figure 6c), while corresponding analysis of the 6 hour subset in 2014 (Figure 7c) yielded differences below 10% 100% of the time regardless of the resolution. ~~When the solar wind density and pressure decrease during 01:00-03:00 UT, July 16, 2012 leading to expansion of the magnetosphere, the difference between the Shue model predictions and GUMICS-4 results grows, with~~ [It should be noted that, despite the relative difference magnitude is slightly lower for the  \$0.5 R\_E\$  resolution run than for the  \$0.25 R\_E\$  resolution run for both the 2012 \(4.9% and 5.6%\) and the 2014 \(0.5\) 3.2% and 4.5%\) events, the  \$0.25 R\_E\$  maximum spatial resolution resulting in](#)

~~67% (58%) within 10% of run reaches better agreement with the Shue model .In comparison, GUMICS-4 results for both resolution runs during the first four hours (July 15, 21:00 UT – especially when the magnetopause is moving during high solar wind driving in July 16, 01:00 UT ) were within 10%. It is thus apparent that using coarse grid (0.5 ) leads to larger difference in magnetopause nose position than using fine grid (0.25 ), if the solar wind density is very low, and the overall driving is relatively strong(Figure 6c).~~

When spatial resolution is increased, gradient quantities such as  $J_Y$  have sharper profiles and therefore larger values Janhunen et al. (2012). As it is the maximum value of  $J_Y$  that we use to locate the magnetopause nose, the nose position evaluation in the lower resolution runs is more ambiguous both due to the larger spread of the current and due to the larger grid cell size. This may lead to changes in the maximum value up to several  $R_E$  over short time periods in response to upstream fluctuations. In the finer resolution runs,  $J_Y$  distribution is sharper, which leads to lesser fluctuations in the maximum value determination. However, the differences between the two grid resolutions occur only under rapidly varying solar wind or very low solar wind density conditions.

The empirical models developed by Shue et al. Shue et al. (1997, 1998) (Shue et al., 1997, 1998) are based on statistical analysis of large number of spacecraft measurements of plasma and magnetic field during magnetopause crossings. While the Shue et al. (1997) model is optimized for moderate upstream conditions, the Shue et al. (1998) targets especially stronger driving periods. However, we computed the difference in the magnetopause position between the two models and found that it is mostly less than  $0.1 R_E$  with maximum difference of  $0.4 R_E$ , with Shue et al. (1997) model predicting more sunward magnetopause nose. Because of the small difference at the magnetopause nose, we have only used Shue et al. (1997) model in our study. Our results agree with previous papers (Palmroth et al., 2003; Lakka et al., 2017), with the latter reporting 3.4% average relative difference between the Shue model and GUMICS-4. Moreover, according to Gordeev et al. (2015), global MHD models are very close to each other in terms of predicting magnetopause standoff distance.

Differences in the magnetopause location do not necessarily translate into differences in global measures, as can be seen from figures 6d and 7d, which show the time evolution of the energy transferred from the solar wind through the magnetopause surface. The response of the total energy  $E_{tot}$  during both ICME cloud periods is quite similar regardless of the used grid resolution. As an integrated quantity, energy entry is a better indicator of the true physical processes of GUMICS-4 solution and does not suffer from dependence on grid resolution like the maximum  $J_Y$  (Janhunen et al., 2012). Therefore, in analyses of simulation results, it would be better to consider such global integrated quantities, even if they have no direct observational counterparts. This can be seen in figures 6d and 7d, with large differences between GUMICS-4 and the  $\epsilon$ -parameter (Perreault and Akasofu, 1978) in energy transferred from the solar wind into the magnetosphere in both 2012 and 2014. However, standard deviations show that GUMICS-4 reproduces temporal evolution of the  $\epsilon$ -parameter better during low solar wind driving (2014) than during high driving (2012), as the respective SD values are 0.725 and 2.263. Moreover, our results are mostly of the same order of magnitude compared to what was obtained by Palmroth et al. (2003) by using plasma flow streamlines for computing the magnetopause surface from GUMICS-4 results.

In the ionosphere, the cross-polar cap potential value is dependent on the grid resolution, with higher resolution yielding higher polar cap potential values. However, typically, the time evolution is similar for both. For the 2012 event the average  $\delta$  during

July 15, 21:00 UT – July 16, 03:00 UT is 31.2% with 0.5  $R_E$  resolution, while with 0.25  $R_E$  resolution it is 16.3%. The 2014 event features similar trend, as the  $\delta$  values are 70% and 27% for the corresponding 6 hour stages using low and high resolutions. As can be seen in Figure 6e, the difference between the two resolution runs can be up to 30% during the first 4 hours of the 6 hour stage, until the CPCP obtained from the 0.5  $R_E$  resolution run starts to increase and eventually catches the 0.25  $R_E$  resolution run at 03:00 UT. Similar evolution is absent during the ~~2012~~ 2014 event (Figure 7e). In comparison with the PCI index (Ridley and Kihn, 2004), standard deviation is considerably lower for the 2014 event (5.107) than for the 2012 event (15.838). Thus, at least two factors contribute to the ionospheric coupling: Grid resolution and intensity of solar wind driving. Considering that the SD values are clearly higher than e.g. the corresponding energy transfer values, and that the PCI index considers only the northern hemisphere, the PCI index may not provide the most accurate reference for GUMICS-4. However, both considerable difference between GUMICS-4 and the PCI and the dependence on grid resolution agree with previous studies (e.g. Lakka et al., 2018). Moreover, Gordeev et al. (2015) reported differences of order tens of kV between GUMICS-4 and other GMHD models.

The polar cap structure and the distribution of the FAC do not change much in either of the simulations, thus suggesting that the coupling of the magnetosphere and the ionosphere remains relatively constant. As is shown in figures 10a–10b, the region 1 currents are clearly visible, while the region 2 currents get stronger only by enhancing the grid resolution in the MHD region ~~Janhunen et al. (2012)~~ (Janhunen et al., 2012). However, the upstream conditions change considerably from 01:00 to 03:00, with the upstream Alfvén Mach number decreasing from 1.9 to 0.6, suggesting that polar cap potential saturation mechanisms ~~is~~ are likely to take place (Ridley, 2007; Wilder et al., 2015; Lakka et al., 2018). Considering that GUMICS-4 reproduces saturation with both 0.5  $R_E$  (this paper) and 0.25  $R_E$  resolutions (Lakka et al., 2018), it is apparent that the FAC influence on the dayside magnetospheric magnetic field do not contribute to the saturation effect. However, to actually prove it is beyond the scope of the current paper. We therefore conclude that the increase of the CPCP during the 0.5  $R_E$  simulation run is caused by processes outside of the magnetosphere, likely in the magnetosheath, and that GUMICS-4 responds differently to low Alfvén Mach number solar wind depending on grid resolution.

Figures 8 and 9 illustrate the CPCP as a function of the solar wind  $E_Y$  component. Color-coded are the IMF magnitude in figures 8a and 9a, the solar wind speed in figures 8b and 9b, and the upstream Alfvén Mach number in figures 8c and 9c. Nominal solar wind conditions before and after the actual ICME events as well as the ICME sheath and cloud periods are considered separately. We note that only results from the ~~maximum~~ lower spatial resolution (0.25–0.5  $R_E$ ) runs are included in the figures. Consistent with earlier studies, Figure 8 shows saturation of the CPCP during high solar wind driving (see e.g. Shepherd (2007); Russell et al. (2001)): With nominal solar wind conditions or during ICME sheath period the response of the CPCP to the upstream  $E_Y$  is rather linear, while for ICME cloud period the CPCP saturates, when  $E_Y > 5$  mV/m. From Figure 8a it can be seen that the saturation occurs when  $B > 12$  nT and Figure 8b shows that the increase of the CPCP in the linear regime depends on the upstream velocity in such a way that the increase is clearly higher for lower velocity values (cloud event), than for higher velocity values (sheath event and nominal conditions), as suggested by previous statistical (Newell et al., 2008) and numerical (Lopez et al., 2010) studies. The latter study proposes that this is because of the more rapid diversion of

35 the solar wind flow in the pressure gradient dominated magnetosheath under faster solar wind, which leaves a smaller amount of plasma at the magnetic reconnection site.

The saturation of the CPCP is absent in Figure 9 due to the significantly weaker solar wind driving during the 2014 event (the upstream  $E_Y$  is below 4 mV/m). This in turn leads to the upstream Alfvén Mach number to be on average 5.8 during the ICME cloud event. Lavraud and Borovsky (2008) suggests that when the Alfvén Mach number decreases below 4 and  
5 the overall magnetosheath plasma beta ( $p/p_B$ , where  $p$  is the plasma pressure and  $p_B$  the magnetic pressure) below 1, the magnetosheath force balance changes such that plasma flow streamlines are diverted away from the magnetic reconnection merging region in the dayside magnetopause (Lopez et al., 2010), which causes the CPCP saturation. However, the CPCP saturation limit of  $M_A = 4$  is not necessarily the only governing parameter, as there is both observational evidence with large  $M_A$  values (up to 7.3) (Myllys et al., 2016) and simulation results indicating saturation at low but above  $M_A = 1$  values (this  
10 study). Nonetheless, our results suggest that the saturation of the CPCP is dependent on the upstream  $M_A$  in such a way that  $M_A$  needs to be below 4 for the saturation to occur.

An interesting aspect is that the CPCP does not reach its maximum simultaneously with  $E_Y$ , i.e. the CPCP is largest with moderate  $E_Y$  (5–6 mV/m) (see Figure 8). As  $E_Y$  increases to 11 mV/m, the CPCP decreases from 70 kV to 40 kV. This is actually apparent in Figure 1h as well: The absolute values of both  $B_Z$  and  $V_X$  reach their maximum values a few hours  
15 after the onset of the magnetic cloud, which is at 6.54 UT, July 15. However, the CPCP is at that time quite moderate, about 40 kV, and does not reach its maximum until July 16, when both  $B_Z$  and  $V_X$  have already reduced significantly. Thus the CPCP overshoots in Figure 8, a feature that was not observed in a GUMICS-4 study by Lakka et al. (2018) using artificial solar wind input consisting of relatively high density and constant driving parameters.

The performance of GUMICS-4 was put to test by means of comparing the magnetic field magnitude  $|B|$  to in-situ data of  
20 Cluster and Geotail satellites. ~~We conclude that ICME cloud period leads to largest differences in GUMICS-4 values are mostly larger than those measured by either of the two spacecraft. Tables 4 and 5 show the relative difference magnitude in  $|B|$  between measured and in-situ data especially during high solar wind driving. Furthermore, during high driving, the magnetopause location estimates may not be sufficiently accurate to cause differences in~~ for both comparison pairs. Overall,  $\delta$  is lower between GUMICS-4 and Cluster, than between GUMICS-4 and Geotail.

25 During both events,  $|B|$  is increased during ICMEs, especially their magnetic cloud counterparts. During the 2012 ICME sheath both Cluster and Geotail record fluctuating  $|B|$  until the onset of the cloud. Albeit missing sheath in 2014, magnetic field magnitude measured by Cluster fluctuates as well prior to the cloud. At the same time (April 29, 15:00 UT)  $|B|$  measured by Geotail decreases sharply.

Largest  $\delta$  between GUMICS-4 and Cluster during the ~~observed satellite position~~ 2012 event is created during the ICME sheath (59.2%), however, this period creates lowest  $\delta$  when comparing GUMICS-4 and Geotail (41.9%). The difference in  $\delta$  between nominal solar wind conditions and ICME cloud is considerably lower for the 2012 event (61.4% and 66.6%) than for the 2014 event (55% and 79.7%) when comparing GUMICS-4 and Geotail. Similar trend is observable if comparison between GUMICS-4 and Cluster is considered, (37.3% and 52.7% for the 2012 event, 36.5% and 62.9% for the 2014 event) albeit with slightly lower magnitude. Moreover, while  $\delta$  is quite similar regardless of Geotail position with respect to the magnetopause in

both 2012 and 2014, it increases from 34.4% to 60.8% during the 2014 event between GUMICS-4 prediction within/outside and Cluster.

As the relative difference magnitudes  $\delta$  are mostly comparable regardless of which of the two events is considered, yet considerably lower for Cluster than Geotail, it is apparent that  $\delta$  is affected more by the spacecraft orbit and, to a lesser extent, the upstream conditions. This is further manifested by the average  $\delta$  over time the spacecraft spends inside and outside the magnetosphere. In table 5 average  $\delta$  in 2014 when the spacecraft is inside the magnetosphere is 34.4% while the value is 60.8% when Cluster is outside the magnetosphere. Comparison between Geotail and GUMICS-4 suggests the same, with 58.2% (65.1%) average  $\delta$  when the spacecraft is inside (outside) the magnetosphere. Computed standard deviations reveal that, over the entire simulation periods, the temporal evolution of GUMICS-4 magnetic field magnitude predictions is closer to Geotail measurements (2012: SD = 5.476, 2014:SD = 6.564, equatorial orbit) than Cluster measurements (2012: SD = 25.054, 2014: SD = 24.795, polar orbit) for both events. It should be noted that the times when Cluster is closer than  $3.7 R_E$  to Earth are ignored when computing  $\delta$  and SD values due to the inner boundary of the GUMICS-4 MHD region, which is located at  $3.7 R_E$ .

## 6 Conclusions

We conclude that for both events,  $|B|$  predicted by GUMICS-4 is closer to Cluster observations, which feature high magnetic field magnitude outside the plasma sheet. However, the SD values suggest that GUMICS-4 reproduces temporal evolution of  $|B|$  better at Geotail, which is much further away from the Earth than Cluster, and resides mostly in the lobe and on the boundary layer. We also computed standard deviations for Cluster orbit when the S/C is both further and closer than  $5 R_E$  away from the center of the Earth. SD for further than  $5 R_E$  is 22.984 (19.666) for the 2012 (2014) event, while for closer than  $5 R_E$  the SD is 106.337 (104.605) for the 2012 (2014) event. If these calculations are repeated for  $6 R_E$  distance, the SD values are 14.390 (15.282) when the S/C is further in 2012 (2014), and 104.618 (88.423) when the S/C is closer in 2012 (2014). Thus, the temporal evolutions agree better when Cluster is further away from the Earth.

The differences are most likely not caused by grid cell size variations due to the adaptive grid of GUMICS-4, because the average  $\delta$  values over simulated 6-hour stages (see tables 4 and 5) are quite similar for both resolutions. Also, most of the difference is created during the first hours of the 6 hour stage, during which the  $0.25 R_E$  run may not have fully eliminated the effects of simulation initialization, which can prevail hours (Lakka et al., 2017). Moreover, the adaptive grid of GUMICS-4 is enhanced the most near the dayside magnetopause. Both events show signs of increased  $|\delta|$  near the dayside magnetopause (edges of yellow-shaded regions in figures 4 and 5), further manifesting inaccuracies in determining the magnetopause in GUMICS-4.

## 6 Conclusions

The results of this paper can be summarized as follows:

- 25 (1) Enhancing spatial resolution of the magnetosphere in GUMICS-4 affects the accuracy of the determination of the magnetopause subsolar point. ~~Some global~~ Global measures, such as energy transferred from the solar wind into the magnetosphere, are not affected. ~~However, the~~ The cross-polar cap potential can be affected significantly, with up to over factor of 2 difference between simulations using different spatial resolutions for the magnetosphere.
- (2) Our results show signs of cross-polar cap potential saturation during low upstream Alfvén Mach number ~~thus agreeing with~~ previous studies. GUMICS-4 responds differently to low Alfvén Mach number solar wind, which may affect the saturation phenomena. This may lead to grid size effects to polar cap saturation in MHD simulations.
- 30 (3) Overall time evolution of the magnetic field magnitude  $|B|$  ~~observed by Cluster and Geotail is similar to that~~ predicted by GUMICS-4, ~~although~~ agrees observed  $|B|$  better when the magnetic field magnitude is high. GUMICS-4 generally overestimates is generally prone to overestimate the field magnitude. ~~The largest differences emerge during the ICME magnetic~~ cloud, when the solar wind driving is particularly strong Due to inaccuracies in the magnetopause subsolar point determination, comparison between GUMICS-4 and in-situ data should be done cautiously when the spacecraft is near the magnetopause.
- 35

*Data availability.* Solar wind data are freely available from the NASA/GSFC Omniweb server (<https://omniweb.gsfc.nasa.gov/>). Solar energetic particle data are freely available from the NOAA NCEI Space Weather data access (<https://www.ngdc.noaa.gov/stp/satellite/goes/index.html>).

*Competing interests.* The authors declare that they have no conflict of interest.

*Acknowledgements.* The calculations presented above were performed using computer resources within the Aalto University School of Science "Science-IT" project. This project was funded by the Academy of Finland grants #1267087, #288472, and #310444. We acknowledge use of NASA/GSFC's Space Physics Data Facility's OMNIWeb service, and OMNI data. Solar energetic particle data supplied courtesy of ngdc.noaa.gov.

5

## References

- Axford, W. I. and Hines, C. O.: A UNIFYING THEORY OF HIGH-LATITUDE GEOPHYSICAL PHENOMENA AND GEOMAGNETIC STORMS, *Canadian Journal of Physics*, 39, 1433–1464, <https://doi.org/10.1139/p61-172>, <http://dx.doi.org/10.1139/p61-172>, 1961.
- Birn, J., Drake, J. F., Shay, M. A., Rogers, B. N., Denton, R. E., Hesse, M., Kuznetsova, M., Ma, Z. W., Bhattacharjee, A., Otto, A., and Pritchett, P. L.: Geospace Environmental Modeling (GEM) Magnetic Reconnection Challenge, *Journal of Geophysical Research: Space Physics*, 106, 3715–3719, <https://doi.org/10.1029/1999JA900449>, <http://dx.doi.org/10.1029/1999JA900449>, 2001.
- Burlaga, L., Sittler, E., Mariani, F., , and Schwenn, R.: Magnetic loop behind an interplanetary shock: Voyager, Helios, and IMP 8 observations, *Journal of Geophysical Research: Space Physics*, 86, 6673–6684, <https://doi.org/10.1029/JA086iA08p06673>, <https://agupubs.onlinelibrary.wiley.com/doi/abs/10.1029/JA086iA08p06673>, 1981.
- Dungey, J. W.: Interplanetary Magnetic Field and the Auroral Zones, *Phys. Rev. Lett.*, 6, 47–48, <https://doi.org/10.1103/PhysRevLett.6.47>, <http://link.aps.org/doi/10.1103/PhysRevLett.6.47>, 1961.
- Goldstein, R., Neugebauer, M., and Clay, D.: A statistical study of coronal mass ejection plasma flows, *Journal of Geophysical Research: Space Physics*, 103, 4761–4766, <https://doi.org/10.1029/97JA03663>, <https://agupubs.onlinelibrary.wiley.com/doi/abs/10.1029/97JA03663>, 1998.
- Gordeev, E., Sergeev, V., Honkonen, I., Kuznetsova, M., Rastätter, L., Palmroth, M., Janhunen, P., Tóth, G., Lyon, J., and Wiltberger, M.: Assessing the performance of community-available global MHD models using key system parameters and empirical relationships, *Space Weather*, 13, 868–884, <https://doi.org/10.1002/2015SW001307>, <http://dx.doi.org/10.1002/2015SW001307>, 2015SW001307, 2015.
- Gosling, J. T.: Coronal Mass Ejections and Magnetic Flux Ropes in Interplanetary Space, pp. 343–364, American Geophysical Union (AGU), <https://doi.org/10.1029/GM058p0343>, <https://agupubs.onlinelibrary.wiley.com/doi/abs/10.1029/GM058p0343>, 1990.
- Gosling, J. T., Pizzo, V., and Bam, S. J.: Anomalous low proton temperatures in the solar wind following interplanetary shock waves—evidence for magnetic bottles?, *Journal of Geophysical Research*, 78, 2001–2009, <https://doi.org/10.1029/JA078i013p02001>, <https://agupubs.onlinelibrary.wiley.com/doi/abs/10.1029/JA078i013p02001>, 1973.
- Gosling, J. T., McComas, D. J., Phillips, J. L., and Bame, S. J.: Geomagnetic activity associated with earth passage of interplanetary shock disturbances and coronal mass ejections, *Journal of Geophysical Research: Space Physics*, 96, 7831–7839, <https://doi.org/10.1029/91JA00316>, <https://agupubs.onlinelibrary.wiley.com/doi/abs/10.1029/91JA00316>, 1991.
- Hirshberg, J. and Colburn, D. S.: Interplanetary field and geomagnetic variations—a unified view, *Planetary and Space Science*, 17, 1183–1206, [https://doi.org/https://doi.org/10.1016/0032-0633\(69\)90010-5](https://doi.org/https://doi.org/10.1016/0032-0633(69)90010-5), 1969.
- Hirshberg, J., Bame, S. J., and Robbins, D. E.: Solar flares and solar wind helium enrichments: July 1965–July 1967, *Solar Physics*, 23, 467–486, <https://doi.org/10.1007/BF00148109>, <https://doi.org/10.1007/BF00148109>, 1972.
- Honkonen, I., Rastätter, L., Grocott, A., Pulkkinen, A., Palmroth, M., Raeder, J., Ridley, A. J., and Wiltberger, M.: On the performance of global magnetohydrodynamic models in the Earth’s magnetosphere, *Space Weather*, 11, 313–326, <https://doi.org/10.1002/swe.20055>, <http://dx.doi.org/10.1002/swe.20055>, 2013.
- Huttunen, K. E. J. and Koskinen, H. E. J.: Importance of post-shock streams and sheath region as drivers of intense magnetospheric storms and high-latitude activity, *Annales Geophysicae*, 22, 1729–1738, <https://hal.archives-ouvertes.fr/hal-00317357>, 2004.
- Huttunen, K. E. J., Koskinen, H. E. J., and Schwenn, R.: Variability of magnetospheric storms driven by different solar wind perturbations, *Journal of Geophysical Research: Space Physics*, 107, SMP 20–1–SMP 20–8, 2002.

- Janhunen, P. and Huuskonen, A.: A numerical ionosphere-magnetosphere coupling model with variable conductivities, *Journal of Geophysical Research: Space Physics*, 98, 9519–9530, <https://doi.org/10.1029/92JA02973>, <http://dx.doi.org/10.1029/92JA02973>, 1993.
- 10 Janhunen, P., Palmroth, M., Laitinen, T., Honkonen, I., Juusola, L., Facskó, G., and Pulkkinen, T.: The GUMICS-4 global {MHD} magnetosphere–ionosphere coupling simulation, *Journal of Atmospheric and Solar-Terrestrial Physics*, 80, 48 – 59, <https://doi.org/http://dx.doi.org/10.1016/j.jastp.2012.03.006>, <http://www.sciencedirect.com/science/article/pii/S1364682612000909>, 2012.
- Jianpeng, G., Xueshang, F., Jie, Z., Pingbing, Z., and Changqing, X.: Statistical properties and geoefficiency of interplanetary coronal mass ejections and their sheaths during intense geomagnetic storms, *Journal of Geophysical Research: Space Physics*, 115, <https://doi.org/10.1029/2009JA015140>, <https://agupubs.onlinelibrary.wiley.com/doi/abs/10.1029/2009JA015140>, 2010.
- J.L. Lions, G. C.: *Handbook of Numerical Analysis. Solution of Equations in  $R_n$  (Part 3), Techniques of Scientific Computing (Part 3)*, vol. Volume 7, North-Holland, 1 edn., 2000.
- Johnson, J. R. and Cheng, C. Z.: Kinetic Alfvén waves and plasma transport at the magnetopause, *Geophysical Research Letters*, 24, 1423–  
20 1426, <https://doi.org/10.1029/97GL01333>, <http://dx.doi.org/10.1029/97GL01333>, 1997.
- Juusola, L., Facskó, G., Honkonen, I., Janhunen, P., Vanhamäki, H., Kauristie, K., Laitinen, T. V., Milan, S. E., Palmroth, M., Tanskanen, E. I., and Viljanen, A.: Statistical comparison of seasonal variations in the GUMICS-4 global MHD model ionosphere and measurements, *Space Weather*, 12, 582–600, <https://doi.org/10.1002/2014SW001082>, 2014.
- Kilpua, E., Isavnin, A., Vourlidis, A., Koskinen, H., and Rodriguez, L.: On the relationship between interplanetary coronal mass ejections  
25 and magnetic clouds, 31, 1251–1265, 2013.
- Kilpua, E., Koskinen, H. E. J., and Pulkkinen, T. I.: Coronal mass ejections and their sheath regions in interplanetary space, *Living Reviews in Solar Physics*, 14, 5, <https://doi.org/10.1007/s41116-017-0009-6>, <https://doi.org/10.1007/s41116-017-0009-6>, 2017a.
- Kilpua, E. K. J., Balogh, A., von Steiger, R., and Liu, Y. D.: Geoeffective Properties of Solar Transients and Stream Interaction Regions, *Space Science Reviews*, 212, 1271–1314, <https://doi.org/10.1007/s11214-017-0411-3>, <https://doi.org/10.1007/s11214-017-0411-3>, 2017b.
- 30 Koustov, A. V., Khachikjan, G. Y., Makarevich, R. A., and Bryant, C.: On the SuperDARN cross polar cap potential saturation effect, *Annales Geophysicae*, 27, 3755–3764, <https://doi.org/10.5194/angeo-27-3755-2009>, 2009.
- Kubota, Y., Nagatsuma, T., Den, M., Tanaka, T., and Fujita, S.: Polar cap potential saturation during the Bastille Day storm event using global MHD simulation, *Journal of Geophysical Research: Space Physics*, 122, 4398–4409, <https://doi.org/10.1002/2016JA023851>, <http://dx.doi.org/10.1002/2016JA023851>, 2016JA023851, 2017.
- 35 Lakka, A., Pulkkinen, T. I., Dimmock, A. P., Osmane, A., Honkonen, I., Palmroth, M., and Janhunen, P.: The impact on global magnetohydrodynamic simulations from varying initialisation methods: results from GUMICS-4, *Annales Geophysicae*, 35, 907–922, <https://doi.org/10.5194/angeo-35-907-2017>, <https://www.ann-geophys.net/35/907/2017/>, 2017.
- Lakka, A., Pulkkinen, T. I., Dimmock, A. P., Myllyls, M., Honkonen, I., and Palmroth, M.: The Cross-Polar Cap Saturation in GUMICS-4 During High Solar Wind Driving, *Journal of Geophysical Research: Space Physics*, 0, <https://doi.org/10.1002/2017JA025054>, <https://agupubs.onlinelibrary.wiley.com/doi/abs/10.1002/2017JA025054>, 2018.
- 5 Lavraud, B. and Borovsky, J. E.: Altered solar wind-magnetosphere interaction at low Mach numbers: Coronal mass ejections, *Journal of Geophysical Research: Space Physics*, 113, n/a–n/a, <https://doi.org/10.1029/2008JA013192>, <http://dx.doi.org/10.1029/2008JA013192>, a00B08, 2008.

- Lopez, R. E., Bruntz, R., Mitchell, E. J., Wiltberger, M., Lyon, J. G., and Merkin, V. G.: Role of magnetosheath force balance in regulating the dayside reconnection potential, *Journal of Geophysical Research: Space Physics*, 115, n/a–n/a, <https://doi.org/10.1029/2009JA014597>, <http://dx.doi.org/10.1029/2009JA014597>, a12216, 2010.
- 10 Myllys, M., Kilpua, E., Lavraud, B., and Pulkkinen, T. I.: Solar wind-magnetosphere coupling efficiency during ejecta and sheath-driven geomagnetic storms, p. 4378–4396, <https://doi.org/10.1002/2016JA022407>, <http://urn.fi/URN:NBN:fi:aalto-201610124801>, 2016.
- Myllys, M., Kipua, E. K. J., and Lavraud, B.: Interplay of solar wind parameters and physical mechanisms producing the saturation of the cross polar cap potential, *Geophysical Research Letters*, 44, 3019–3027, <https://doi.org/10.1002/2017GL072676>, <https://agupubs.onlinelibrary.wiley.com/doi/abs/10.1002/2017GL072676>, 2017.
- 15 Newell, P. T., Sotirelis, T., Liou, K., and Rich, F. J.: Pairs of solar wind-magnetosphere coupling functions: Combining a merging term with a viscous term works best, *Journal of Geophysical Research: Space Physics*, 113, n/a–n/a, <https://doi.org/10.1029/2007JA012825>, <http://dx.doi.org/10.1029/2007JA012825>, a04218, 2008.
- Nishida, A.: Coherence of geomagnetic DP 2 fluctuations with interplanetary magnetic variations, *Journal of Geophysical Research*, 73, 20 5549–5559, <https://doi.org/10.1029/JA073i017p05549>, <http://dx.doi.org/10.1029/JA073i017p05549>, 1968.
- Nykyri, K. and Otto, A.: Plasma transport at the magnetospheric boundary due to reconnection in Kelvin-Helmholtz vortices, *Geophysical Research Letters*, 28, 3565–3568, <https://doi.org/10.1029/2001GL013239>, <http://dx.doi.org/10.1029/2001GL013239>, 2001.
- Osmane, A., Dimmock, A., Naderpour, R., Pulkkinen, T., and Nykyri, K.: The impact of solar wind ULF B-z fluctuations on geomagnetic activity for viscous timescales during strongly northward and southward IMF, *JOURNAL OF GEOPHYSICAL RESEARCH: SPACE* 25 *PHYSICS*, 120, 9307–9322, <https://doi.org/10.1002/2015JA021505>, 2015.
- Palmroth, M., Pulkkinen, T. I., Janhunen, P., and Wu, C.-C.: Stormtime energy transfer in global MHD simulation, *Journal of Geophysical Research: Space Physics*, 108, n/a–n/a, <https://doi.org/10.1029/2002JA009446>, <http://dx.doi.org/10.1029/2002JA009446>, 1048, 2003.
- Perreault, P. and Akasofu, S.-I.: A study of geomagnetic storms, *Geophysical Journal of the Royal Astronomical Society*, 54, 547–573, 1978.
- Pulkkinen, A., Kuznetsova, M., Ridley, A., Raeder, J., Vapirev, A., Weimer, D., Weigel, R. S., Wiltberger, M., Millward, G., Rastätter, L., 30 Hesse, M., Singer, H. J., and Chulaki, A.: Geospace Environment Modeling 2008–2009 Challenge: Ground magnetic field perturbations, *Space Weather*, 9, n/a–n/a, <https://doi.org/10.1029/2010SW000600>, <http://dx.doi.org/10.1029/2010SW000600>, s02004, 2011.
- Pulkkinen, T. I., Partamies, N., Huttunen, K. E. J., Reeves, G. D., and Koskinen, H. E. J.: Differences in geomagnetic storms driven by magnetic clouds and ICME sheath regions, *Geophysical Research Letters*, 34, <https://doi.org/10.1029/2006GL027775>, <https://agupubs.onlinelibrary.wiley.com/doi/abs/10.1029/2006GL027775>, 2007.
- 35 Richardson, I. G. and Cane, H. V.: Identification of interplanetary coronal mass ejections at 1 AU using multiple solar wind plasma composition anomalies, *Journal of Geophysical Research: Space Physics*, 109, <https://doi.org/10.1029/2004JA010598>, <https://agupubs.onlinelibrary.wiley.com/doi/abs/10.1029/2004JA010598>, 2003.
- Richardson, I. G. and Cane, H. V.: Solar wind drivers of geomagnetic storms during more than four solar cycles, *J. Space Weather Space Clim.*, 2, A01, <https://doi.org/10.1051/swsc/2012001>, <https://doi.org/10.1051/swsc/2012001>, 2012.
- Ridley, A. J.: A new formulation for the ionospheric cross polar cap potential including saturation effects, *Annales Geophysicae*, 23, 3533–3547, <https://hal.archives-ouvertes.fr/hal-00318077>, 2005.
- Ridley, A. J.: Alfvén wings at Earth’s magnetosphere under strong interplanetary magnetic fields, *Annales Geophysicae*, 25, 533–542, <https://doi.org/10.5194/angeo-25-533-2007>, <http://www.ann-geophys.net/25/533/2007/>, 2007.

- Ridley, A. J. and Kihn, E. A.: Polar cap index comparisons with AMIE cross polar cap potential, electric field, and polar cap area, *Geophysical Research Letters*, 31, <https://doi.org/10.1029/2003GL019113>, <https://agupubs.onlinelibrary.wiley.com/doi/abs/10.1029/2003GL019113>, 2004.
- Russell, C. T., Luhmann, J. G., and Lu, G.: Nonlinear response of the polar ionosphere to large values of the interplanetary electric field, *Journal of Geophysical Research: Space Physics*, 106, 18 495–18 504, <https://doi.org/10.1029/2001JA900053>, <http://dx.doi.org/10.1029/2001JA900053>, 2001.
- Shepherd, S. G.: Polar cap potential saturation: Observations, theory, and modeling, *Journal of Atmospheric and Solar-Terrestrial Physics*, 69, 234–248, 2007.
- Shue, J.-H., Chao, J. K., Fu, H. C., Russell, C. T., Song, P., Khurana, K. K., and Singer, H. J.: A new functional form to study the solar wind control of the magnetopause size and shape, *Journal of Geophysical Research: Space Physics*, 102, 9497–9511, <https://doi.org/10.1029/97JA00196>, <http://dx.doi.org/10.1029/97JA00196>, 1997.
- Shue, J.-H., Song, P., Russell, C. T., Steinberg, J. T., Chao, J. K., Kokubun, S., Singer, H. J., Detman, T. R., Zastenker, G., Vaisberg, O. L., and Kawano, H.: Magnetopause location under extreme solar wind conditions, *Journal of Geophysical Research: Space Physics*, 103, 17 691–17 700, <https://doi.org/10.1029/98JA01103>, <https://agupubs.onlinelibrary.wiley.com/doi/abs/10.1029/98JA01103>, 1998.
- Siscoe, G. L., Lotko, W., and Sonnerup, B. U.: A high-latitude, low-latitude boundary layer model of the convection current system, *Journal of Geophysical Research: Space Physics*, 96, 3487–3495, 1991.
- Tanaka, T.: Finite Volume TVD Scheme on an Unstructured Grid System for Three-Dimensional MHD Simulation of Inhomogeneous Systems Including Strong Background Potential Fields, *Journal of Computational Physics*, 111, 381 – 389, <https://doi.org/http://dx.doi.org/10.1006/jcph.1994.1071>, <http://www.sciencedirect.com/science/article/pii/S0021999184710710>, 1994.
- Tsurutani, B. T., Gonzalez, W. D., Tang, F., Akasofu, S. I., and Smith, E. J.: Origin of interplanetary southward magnetic fields responsible for major magnetic storms near solar maximum (1978–1979), *Journal of Geophysical Research: Space Physics*, 93, 8519–8531, <https://doi.org/10.1029/JA093iA08p08519>, <https://agupubs.onlinelibrary.wiley.com/doi/abs/10.1029/JA093iA08p08519>, 1988.
- Wilder, F. D., Clauer, C. R., Baker, J. B. H., Cousins, E. P., and Hairston, M. R.: The nonlinear response of the polar cap potential under southward IMF: A statistical view, *Journal of Geophysical Research: Space Physics*, 116, n/a–n/a, <https://doi.org/10.1029/2011JA016924>, <http://dx.doi.org/10.1029/2011JA016924>, a12229, 2011.
- Wilder, F. D., Eriksson, S., and Wiltberger, M.: The role of magnetic flux tube deformation and magnetosheath plasma beta in the saturation of the Region 1 field-aligned current system, *Journal of Geophysical Research: Space Physics*, 120, 2036–2051, <https://doi.org/10.1002/2014JA020533>, <http://dx.doi.org/10.1002/2014JA020533>, 2014JA020533, 2015.
- Wu, C.-C., Fry, C. D., Wu, S. T., Dryer, M., and Liou, K.: Three-dimensional global simulation of interplanetary coronal mass ejection propagation from the Sun to the heliosphere: Solar event of 12 May 1997, *Journal of Geophysical Research: Space Physics*, 112, <https://doi.org/10.1029/2006JA012211>, <https://agupubs.onlinelibrary.wiley.com/doi/abs/10.1029/2006JA012211>, 2007.
- Wu, C.-C., Liou, K., Vourlidas, A., Plunkett, S., Dryer, M., Wu, S. T., and Mewaldt, R. A.: Global magnetohydrodynamic simulation of the 15 March 2013 coronal mass ejection event—Interpretation of the 30–80 MeV proton flux, *Journal of Geophysical Research: Space Physics*, 121, 56–76, <https://doi.org/10.1002/2015JA021051>, <https://agupubs.onlinelibrary.wiley.com/doi/abs/10.1002/2015JA021051>, 2015.
- Yermolaev, Y. I., Nikolaeva, N. S., Lodkina, I. G., and Yermolaev, M. Y.: Geoeffectiveness and efficiency of CIR, sheath, and ICME in generation of magnetic storms, *Journal of Geophysical Research: Space Physics*, 117, <https://doi.org/10.1029/2011JA017139>, <https://agupubs.onlinelibrary.wiley.com/doi/abs/10.1029/2011JA017139>, 2012.

755 Zhang, J., Poomvises, W., and Richardson, I. G.: Sizes and relative geoeffectiveness of interplanetary coronal mass ejections and the preceding shock sheaths during intense storms in 1996–2005, *Geophysical Research Letters*, 35, <https://doi.org/10.1029/2007GL032045>, <https://agupubs.onlinelibrary.wiley.com/doi/abs/10.1029/2007GL032045>, 2012.

**Table 1.** Summary of the event simulations within the current study.

Event year	Nominal solar wind [h]	Event date and time	Event length [h]	Resolution [ $R_E$ ]
2012	9.9	18:53 UT, July 14 – 04:19 UT, July 17	57.4	0.5
2014	25.6	20:38 UT, April 29 – 17:51 UT, April 30	21.2	0.5
2012	0	21:00 UT, July 15 – 03:00 UT, July 16	6	0.25
2014	0	00:00 UT, April 30 – 06:00 UT, April 30	6	0.25

**Table 2.** Average relative difference magnitudes in the magnetopause nose position for given simulation phase.

<u>Event year</u>	<u>Resolution [<math>R_E</math>]</u>	<u>Nominal SW [%]</u>	<u>Sheath [%]</u>	<u>Cloud [%]</u>	<u>6 hours [%]</u>
<u>2012</u>	<u>0.5</u>	<u>2.5</u>	<u>4.5</u>	<u>8.0</u>	<u>4.9</u>
<u>2014</u>	<u>0.5</u>	<u>2.4</u>	<u>~</u>	<u>3.3</u>	<u>3.2</u>
<u>2012</u>	<u>0.25</u>	<u>~</u>	<u>~</u>	<u>~</u>	<u>5.6</u>
<u>2014</u>	<u>0.25</u>	<u>~</u>	<u>~</u>	<u>~</u>	<u>4.5</u>

~~The calculations presented above were performed using computer resources within the Aalto University School of Science "Science-IT" project. This project was funded by the Academy of Finland grants #288472 and #267073/2013. We acknowledge use of NASA/GSFC's Space Physics Data Facility's OMNIWeb service, and OMNI data.~~

760

**Table 3.** Average relative difference magnitudes in the cross-polar cap potential for given simulation phase.

<u>Event year</u>	<u>Resolution [R<sub>E</sub>]</u>	<u>Nominal SW [%]</u>	<u>Sheath [%]</u>	<u>Cloud [%]</u>	<u>6 hours [%]</u>
<u>2012</u>	<u>0.5</u>	<u>64.9</u>	<u>57.6</u>	<u>36.0</u>	<u>31.2</u>
<u>2014</u>	<u>0.5</u>	<u>46.9</u>	<u>~</u>	<u>69.2</u>	<u>70.0</u>
<u>2012</u>	<u>0.25</u>	<u>~</u>	<u>~</u>	<u>~</u>	<u>16.3</u>
<u>2014</u>	<u>0.25</u>	<u>~</u>	<u>~</u>	<u>~</u>	<u>27.0</u>

**Table 4.** Geotail vs. GUMICS-4: Average relative difference magnitudes in the magnetic field magnitude for given simulation phase. SC inside/outside refers to sequences during which the spacecraft is inside/outside the magnetosphere according to figure 3.

<u>Event year</u>	<u>Resolution [R<sub>E</sub>]</u>	<u>Nominal SW [%]</u>	<u>Sheath [%]</u>	<u>Cloud [%]</u>	<u>SC inside [%]</u>	<u>SC outside [%]</u>	<u>6 hours [%]</u>
<u>2012</u>	<u>0.5</u>	<u>61.4</u>	<u>41.9</u>	<u>66.6</u>	<u>61.1</u>	<u>62.7</u>	<u>69.7</u>
<u>2014</u>	<u>0.5</u>	<u>55.0</u>	<u>~</u>	<u>79.7</u>	<u>58.2</u>	<u>65.1</u>	<u>80.5</u>
<u>2012</u>	<u>0.25</u>	<u>~</u>	<u>~</u>	<u>~</u>	<u>~</u>	<u>~</u>	<u>68.2</u>
<u>2014</u>	<u>0.25</u>	<u>~</u>	<u>~</u>	<u>~</u>	<u>~</u>	<u>~</u>	<u>64.8</u>

**Table 5.** Cluster vs. GUMICS-4: Average relative difference magnitudes in the magnetic field magnitude for given simulation phase. SC inside/outside refers to sequences during which the spacecraft is inside/outside the magnetosphere according to figure 3.

<u>Event year</u>	<u>Resolution [R<sub>E</sub>]</u>	<u>Nominal SW [%]</u>	<u>Sheath [%]</u>	<u>Cloud [%]</u>	<u>SC inside [%]</u>	<u>SC outside [%]</u>	<u>6 hours [%]</u>
<u>2012</u>	<u>0.5</u>	<u>37.3</u>	<u>59.2</u>	<u>52.7</u>	<u>49.7</u>	<u>~</u>	<u>58.6</u>
<u>2014</u>	<u>0.5</u>	<u>36.5</u>	<u>~</u>	<u>62.9</u>	<u>34.4</u>	<u>60.8</u>	<u>49.7</u>
<u>2012</u>	<u>0.25</u>	<u>~</u>	<u>~</u>	<u>~</u>	<u>~</u>	<u>~</u>	<u>53.0</u>
<u>2014</u>	<u>0.25</u>	<u>~</u>	<u>~</u>	<u>~</u>	<u>~</u>	<u>~</u>	<u>50.0</u>

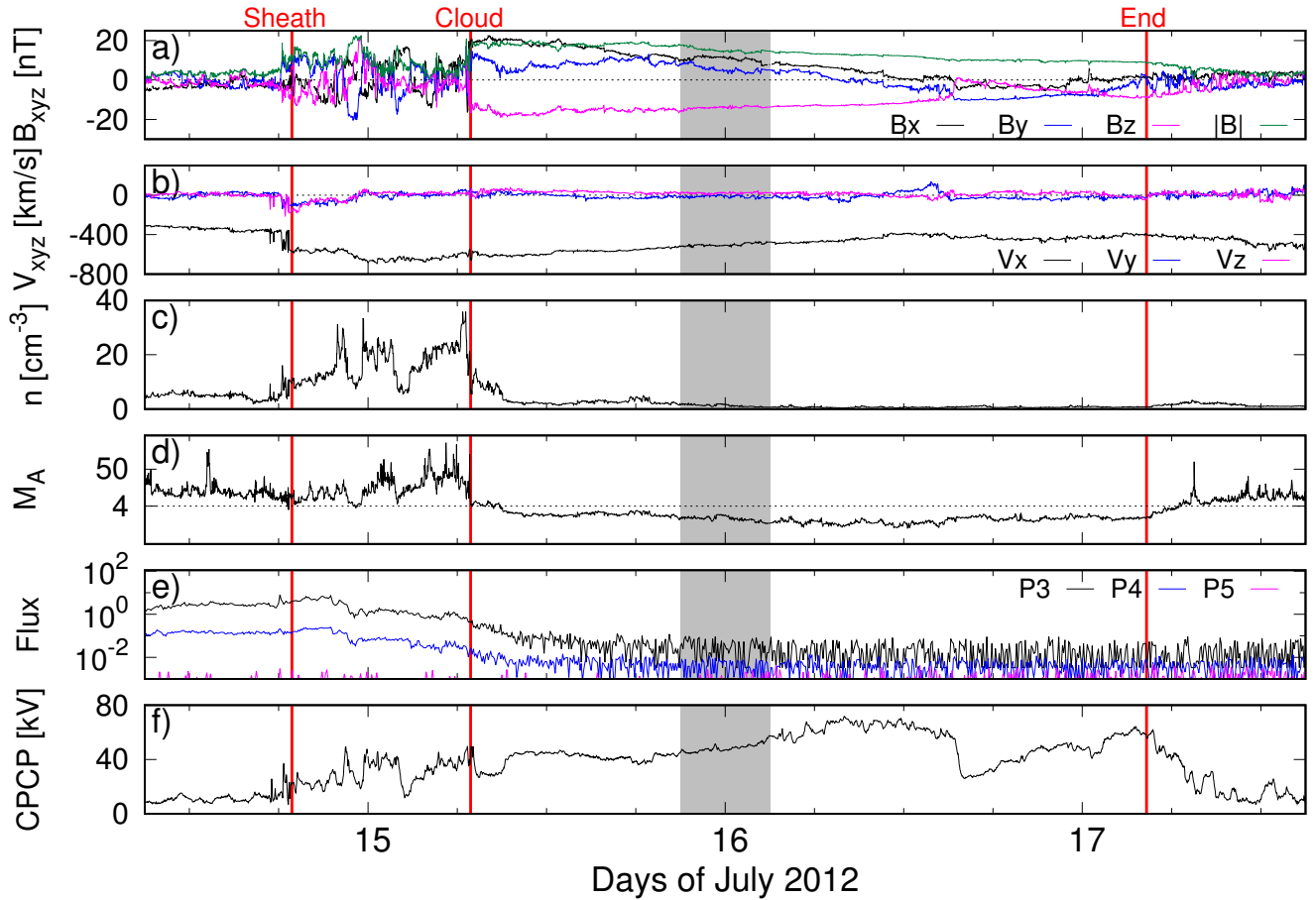


**Figure 1.** Solar wind and IMF conditions during July 14 09:00 UT – July 17 15:00 UT, 2012. Panels from top to bottom: a) IMF components  $B_X$ ,  $B_Y$  and  $B_Z$  and the IMF magnitude in nT, b) plasma velocity components  $V_X$ ,  $V_Y$  and  $V_Z$  in km/s, c) plasma number density  $n$  in  $\text{cm}^{-3}$ , d) upstream Alfvén Mach number  $M_A$  ( $M_A = 4$  is marked with dotted line), e) [GOES-15 geostationary orbit](#) proton fluxes for three energy channels between 8–80 MeV, and f) the [ionospheric](#) cross-polar cap potential from GUMICS-4. [Data in panels a–d is measured by ACE/Wind.](#) Vertical red lines indicate onset of the ICME sheath/magnetic cloud or the end of the ICME event. Grey background shows [which the](#) part of the ICME event [that](#) is simulated using both 0.25 and 0.5  $R_E$  as a maximum spatial resolution.

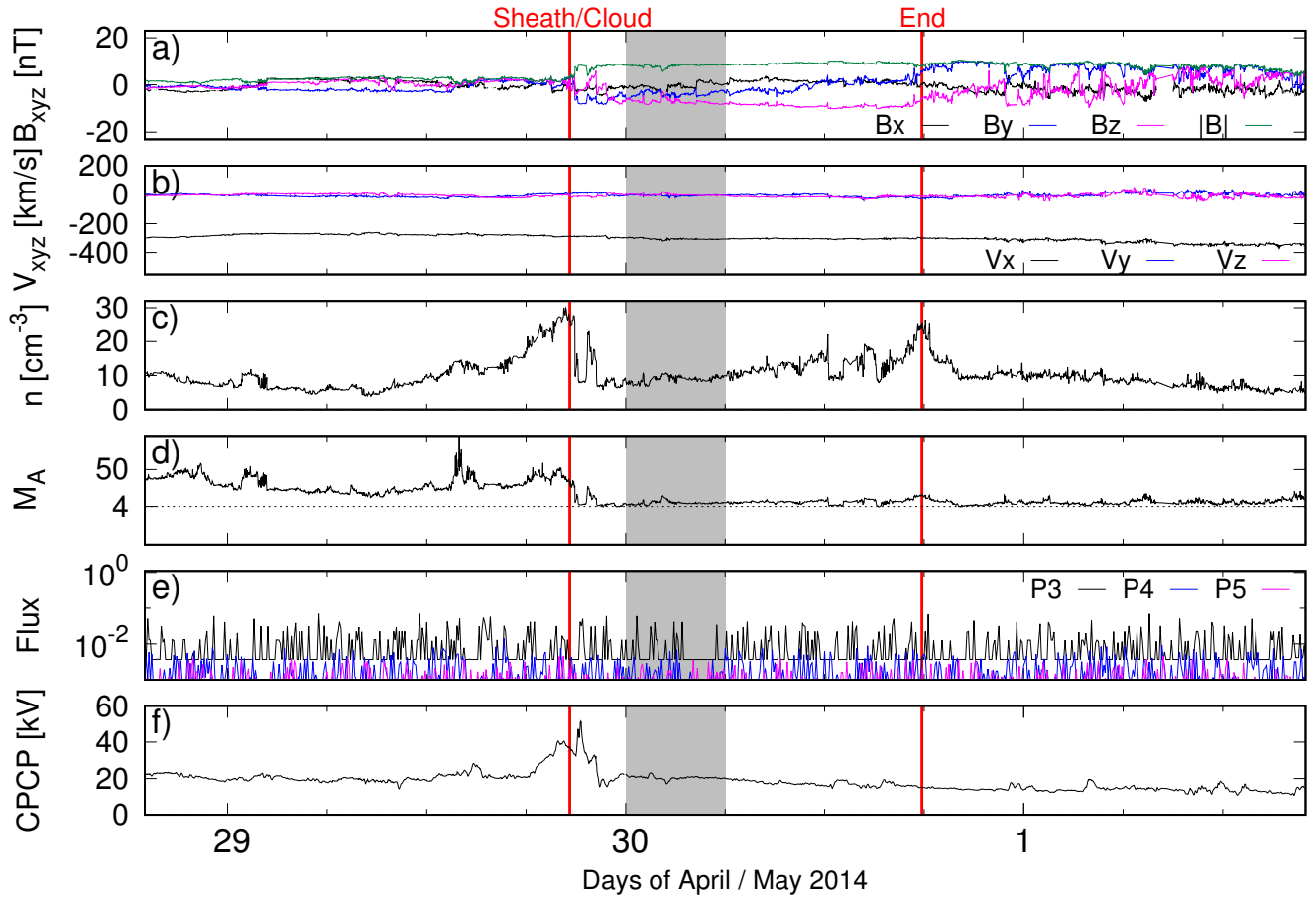


**Figure 2.** Solar wind and IMF conditions during April 28 19:00 UT – May 1 17:00 UT, 2014. Panels from top to bottom: a) IMF components  $B_X$ ,  $B_Y$  and  $B_Z$  and the IMF magnitude in nT, b) plasma velocity components  $V_X$ ,  $V_Y$  and  $V_Z$  in km/s, c) plasma number density  $n$  in  $\text{cm}^{-3}$ , d) upstream Alfvén Mach number  $M_A$  ( $M_A = 4$  is marked with dotted line), e) [GOES-15 geostationary orbit](#) proton fluxes for three energy channels between 8–80 MeV, and f) the [ionospheric](#) cross-polar cap potential from GUMICS-4. [Data in panels a–d is measured by ACE/Wind.](#) Vertical red lines indicate onset of the ICME sheath/magnetic cloud or the end of the ICME event. Grey background shows [which the](#) part of the ICME event [that](#) is simulated using both  $0.25$  and  $0.5 R_E$  as a maximum spatial resolution.

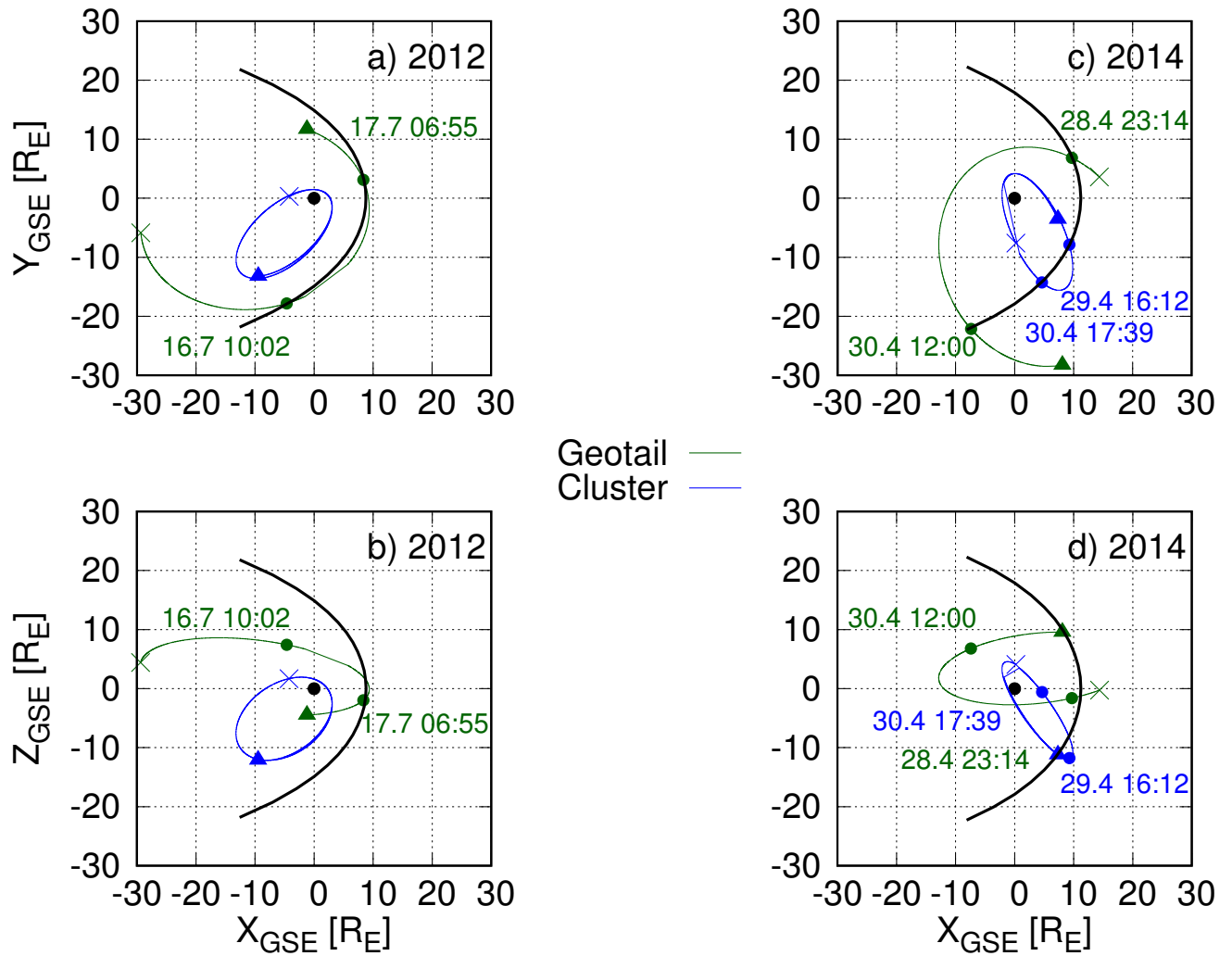


**Figure 3.** Orbits of Cluster 1 (blue) and Geotail (magenta-green) satellites during July 14 09:00 UT – July 17 15:00 UT, 2012 (panels a and b) and during April 28 19:00 UT – May 1 17:00 UT, 2014 (panels c and d). Orbits are shown on the  $XY$  plane in panels a and c and on the  $XZ$  plane in panels b and d. The used coordinate system is GSE. The most earthward occurrence position of the Shue magnetopause during both time intervals is drawn with-in black. Starting Start and ending-end points of the time intervals under-inspections are marked with a cross and a triangle, respectively, while the approximate. The points where-along the satellite orbits intersect-between which the spacecraft may encounter magnetopause crossings are marked with dots.

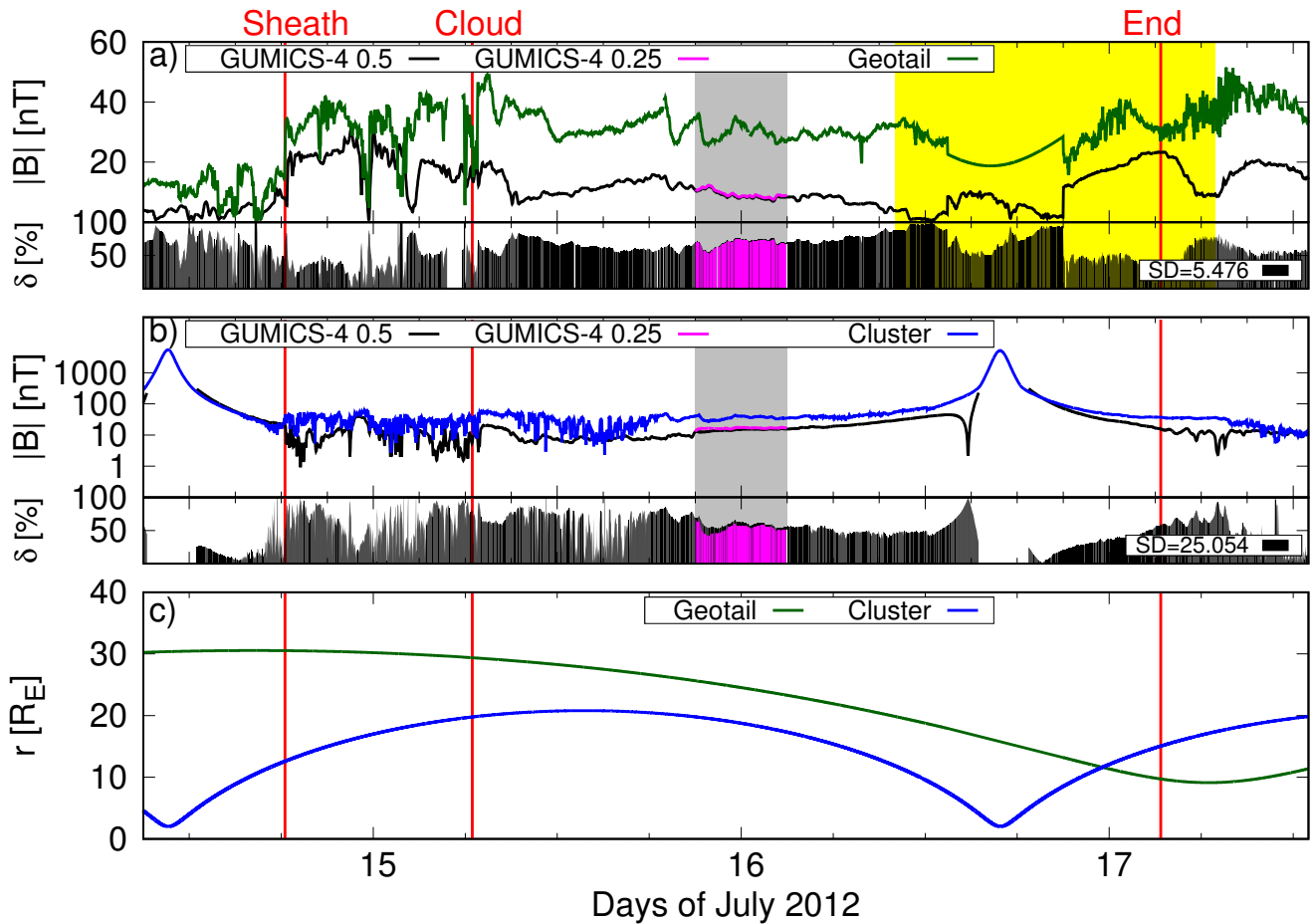


**Figure 4.** The time series of the magnetic field magnitude  $|B|$  along the orbits of Geotail (panel a) and Cluster 1 (panel b) during July 14 09:00 UT – July 17 15:00 UT, 2012 as measured by the two satellites (Geotail as magenta (green) and Cluster 1 as (blue) and predicted by GUMICS-4 (black and magenta). Black and magenta curves in panels a–b show GUMICS-4 results with maximum spatial resolution of 0.5 (black) and 0.25 (magenta)  $R_E$ . Panel c: Radial distance of both spacecraft from the center of the Earth. Grey-shaded-The relative difference magnitude in  $|B|$  between GUMICS-4 and the observation is given in panels a and b. Yellow-shaded regions indicate approximate time intervals when satellite is outside may exit the magnetosphere. Grey-shaded regions show the part of the ICME event simulated also using 0.25  $R_E$  maximum spatial resolution. Standard deviations (SD) for observation vs. GUMICS-4 (0.5  $R_E$  resolution) datasets are given in panels a and b.

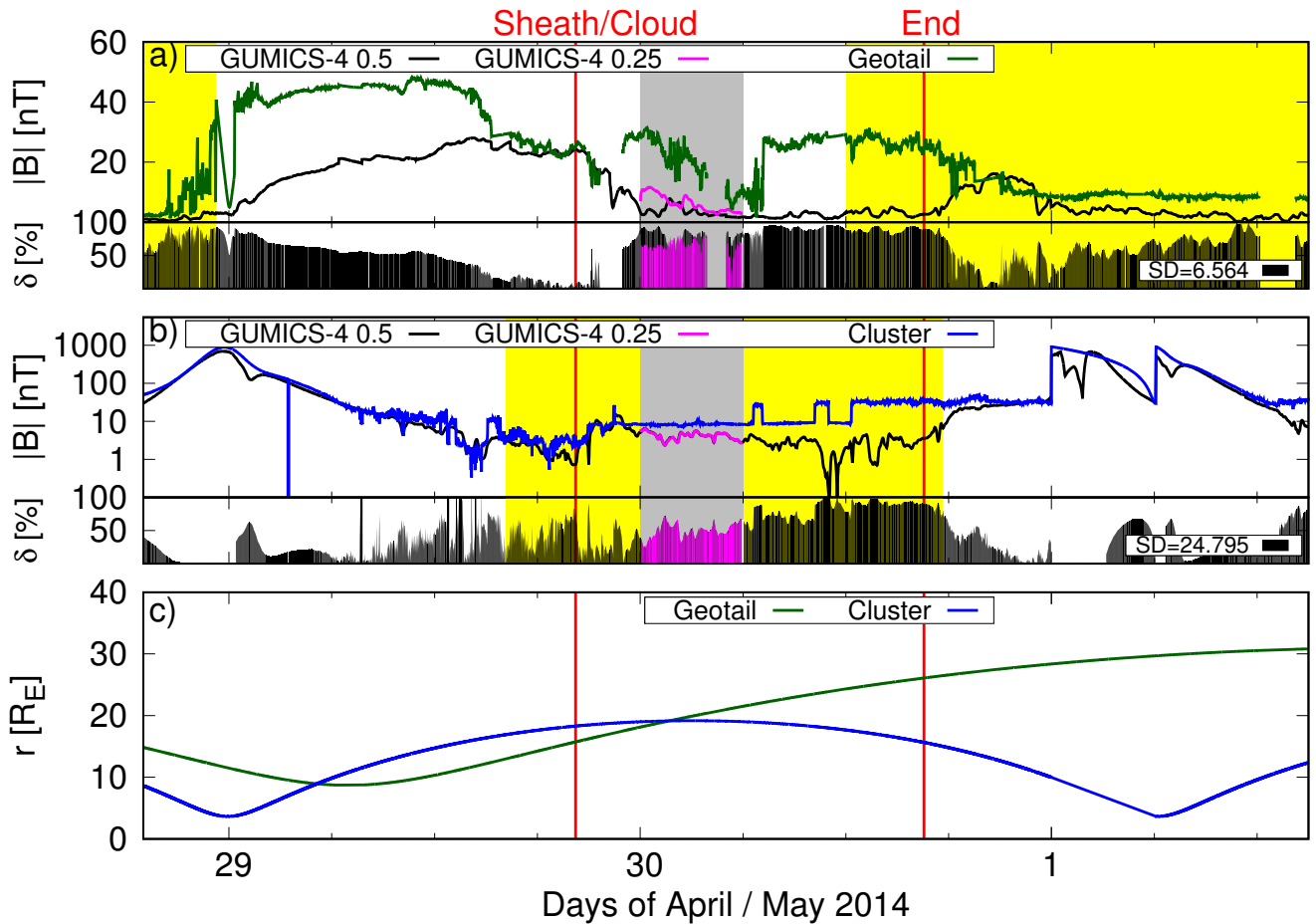


**Figure 5.** The time series of the magnetic field magnitude  $|B|$  along the orbits of Geotail (panel a) and Cluster 1 (panel b) during April 28 19:00 UT – May 1 17:00 UT, 2014 as measured by the two satellites (Geotail as magenta (green) and Cluster 1 as (blue) and predicted by GUMICS-4 (black and magenta). Black and magenta curves in panels a–b show GUMICS-4 results with maximum spatial resolution of 0.5 (black) and 0.25 (magenta)  $R_E$ . Panel c: Radial distance of both spacecraft from the center of the Earth. Grey-shaded-The relative difference magnitude in  $|B|$  between GUMICS-4 and the observation is given in panels a and b. Yellow-shaded regions indicate approximate time intervals when satellite is outside may exit the magnetosphere. Grey-shaded regions show the part of the ICME event simulated also using 0.25  $R_E$  maximum spatial resolution. Standard deviations (SD) for observation vs. GUMICS-4 (0.5  $R_E$  resolution) datasets are given in panels a and b.

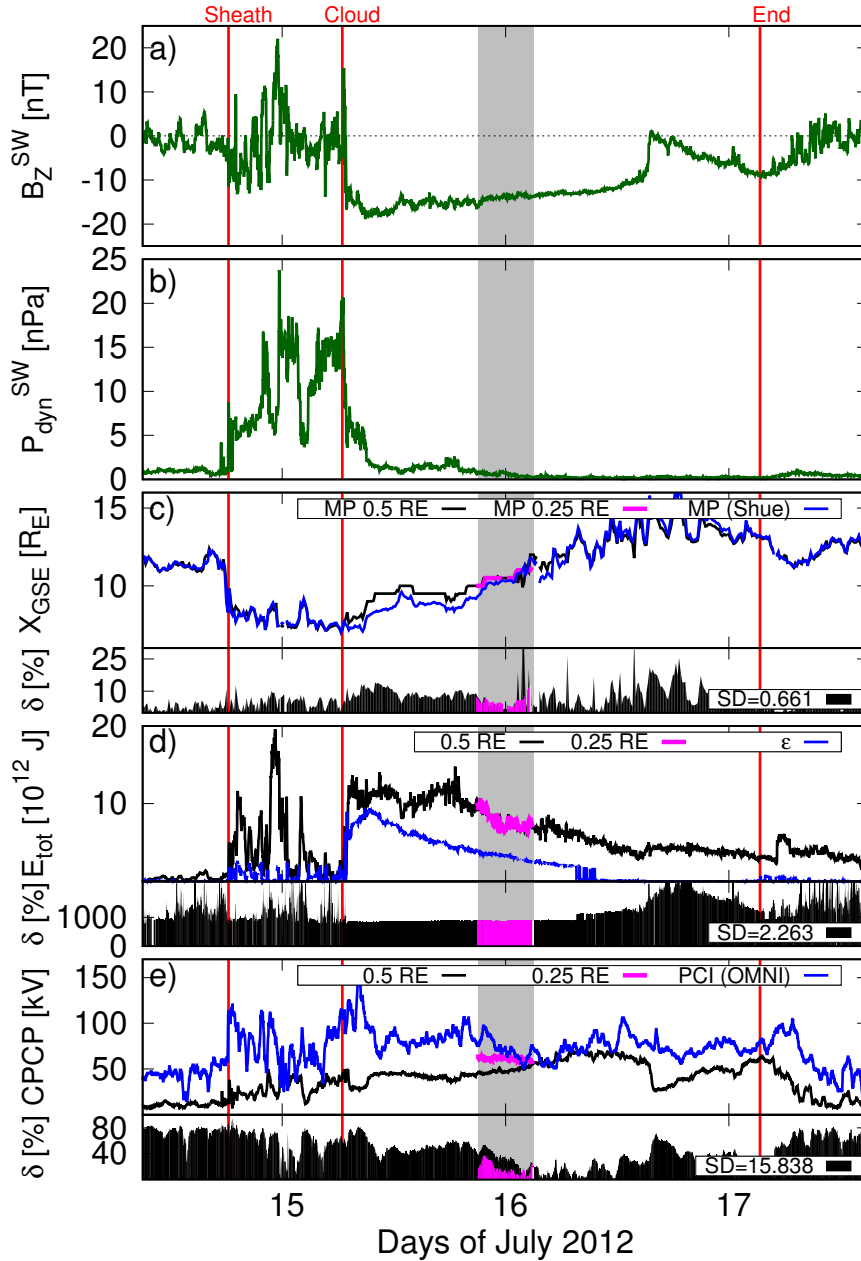


**Figure 6.** a) Interplanetary magnetic field  $z$ -component  $Z$ -component, b) solar wind dynamic pressure, c) [distance to the nose of the magnetopause](#), d) [energy transferred from the solar wind into the magnetosphere through the dayside magnetopause](#), and e) [the cross-polar cap potential](#) during July 15 21:00 UT - July 16 03:00 UT, 2012. [Black and magenta](#) [Magenta](#) plots in panels c-d [imply which show results with maximum spatial resolution is used \(0.5 \(black\) and of 0.25 \(magenta\)  \$R\_E\$ \)](#). [Blue plot curves in panel panels c marks-, d, and e show the magnetopause nose computed using reference values \(the Shue model, the  \$\epsilon\$ -parameter, the PCI index\)](#). [The relative difference magnitude  \$\delta\$  between GUMICS-4 and the reference value is shown in panels c-e](#). [Standard deviations \(SD\) for reference vs. GUMICS-4 \(0.5  \$R\_E\$  resolution\) datasets are given in panels c-e](#).

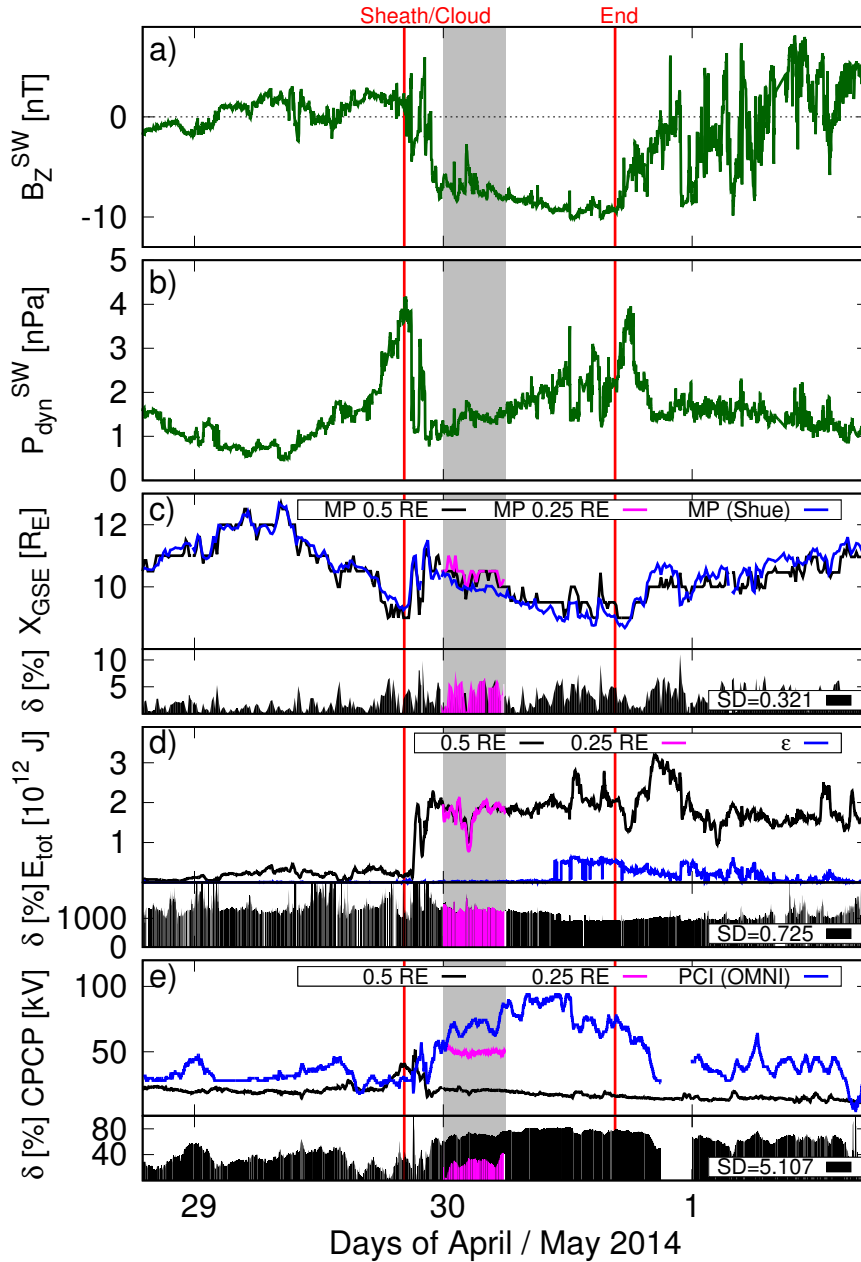


**Figure 7.** a) Interplanetary magnetic field  $z$ -component  $Z$ -component, b) solar wind dynamic pressure, c) [distance to the nose of the magnetopause](#), d) energy transferred from the solar wind into the magnetosphere through the dayside magnetopause, and e) the cross-polar cap potential during April 30 00:00 UT – 06:00 UT, 2014. [Black and magenta Magenta plots in panels c–d imply which show results with maximum spatial resolution is used \(0.5 \(black\) and of 0.25 \(magenta\)  \$R\_E\$ \)](#). [Blue plot curves in panel panels c marks-, d, and e show the magnetopause nose computed using reference values \(the Shue model, the  \$\epsilon\$ -parameter, the PCI index\)](#). [The relative difference magnitude  \$\delta\$  between GUMICS-4 and the reference value is shown in panels c–e](#). [Standard deviations \(SD\) for reference vs. GUMICS-4 \(0.5  \$R\_E\$  resolution\) datasets are given in panels c–e](#).

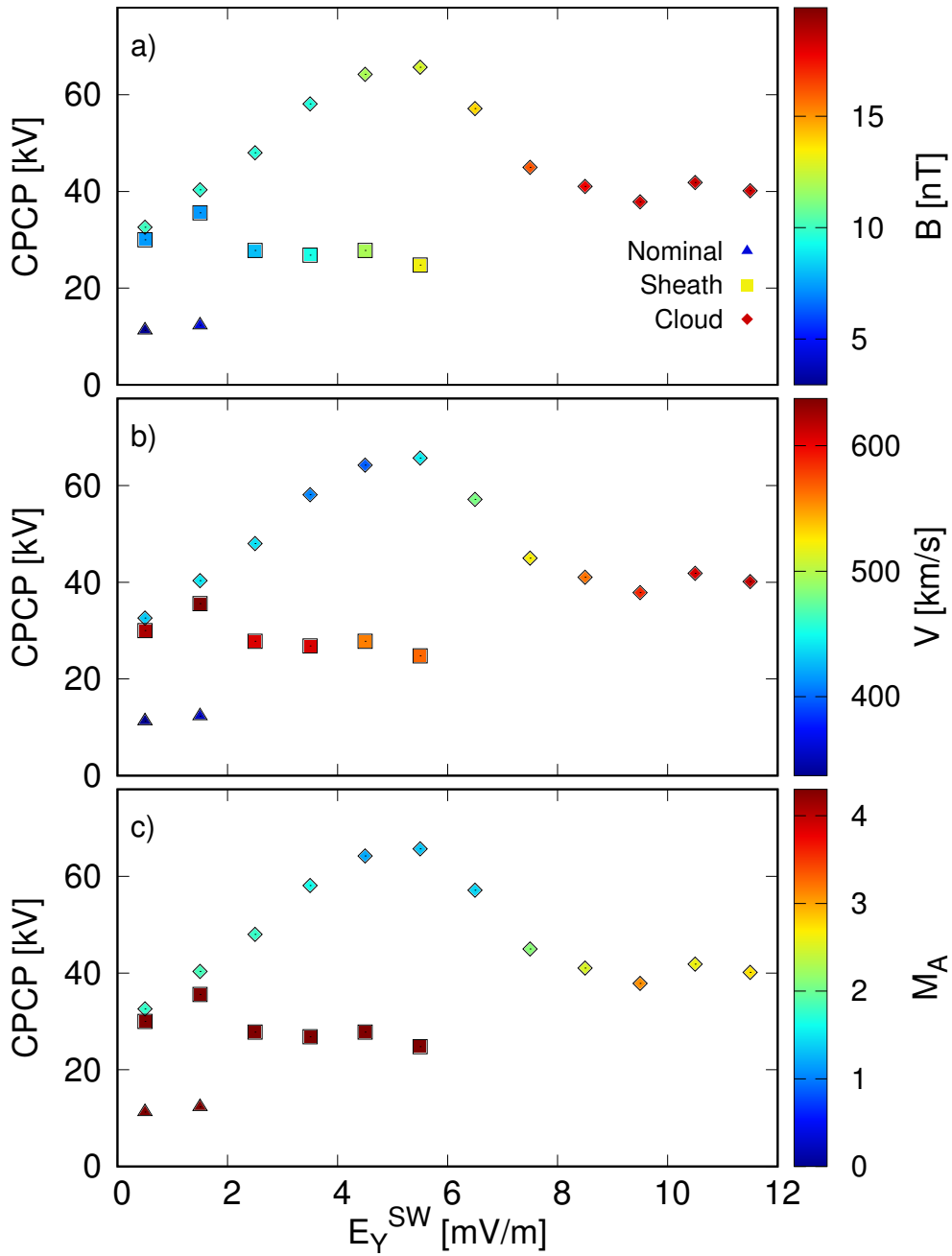


**Figure 8.** The cross-polar cap potential (CPCP) as a function of the IMF  $E_Y$  for the 2012 ICME sheath and cloud periods, with nominal solar wind conditions before and after the ICME event taken into account separately. GUMICS-4 simulation data with 1 minute time resolution has been averaged by 10 minutes and binned by upstream  $E_Y$  with 1.0 mV/m intervals. Panels a, b and c are showing show the magnitudes of the IMF, the upstream flow speed and the Alfvén Mach number, respectively.

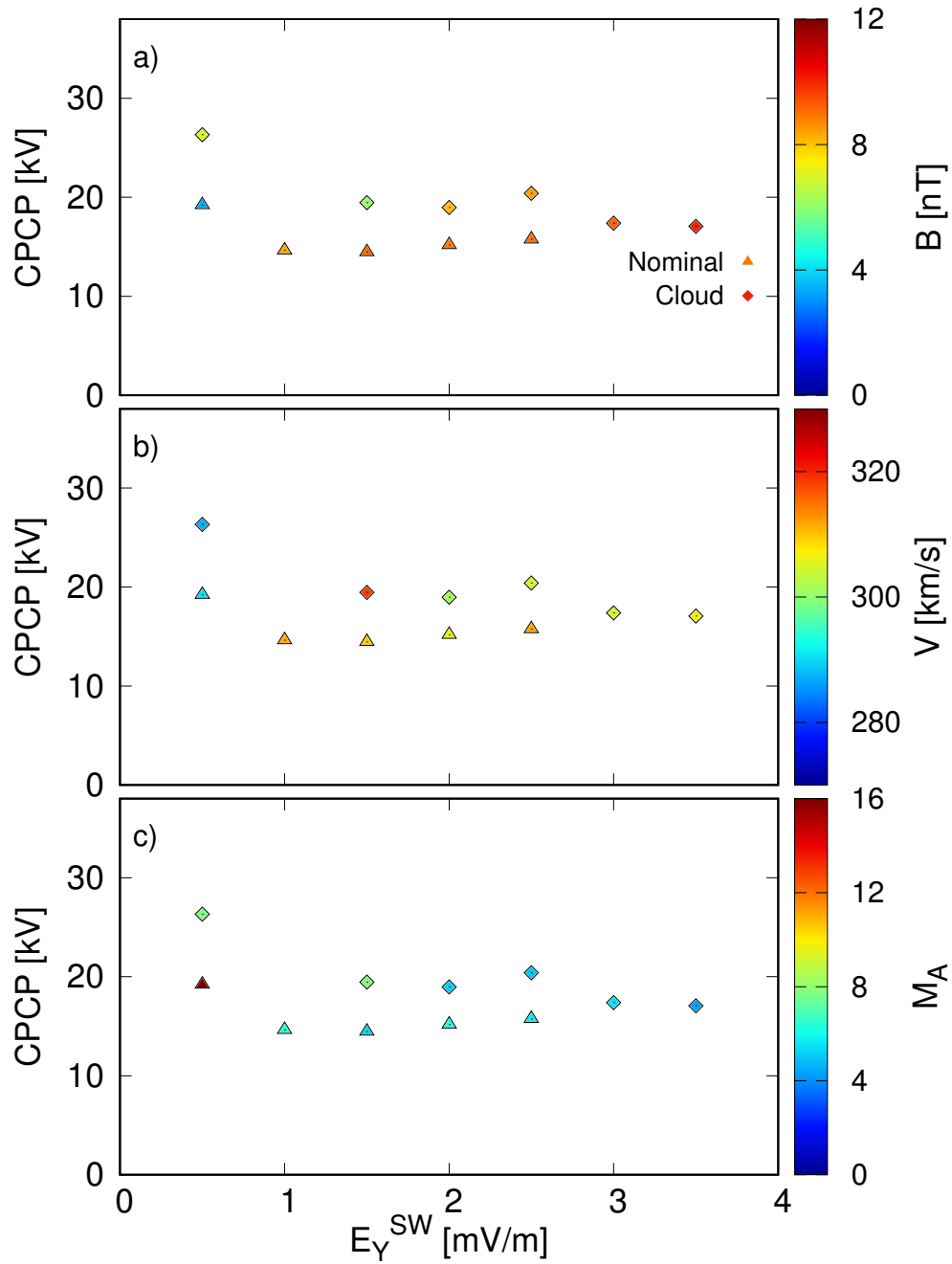
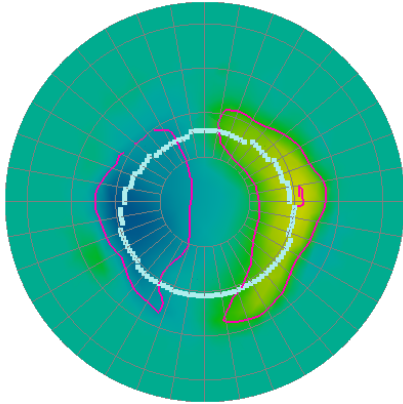
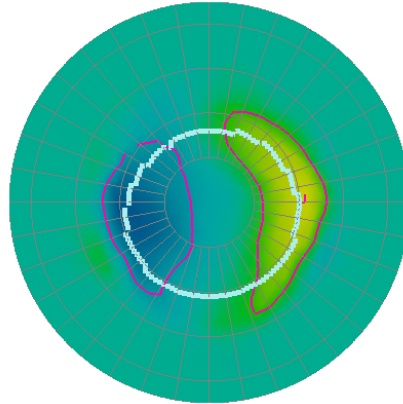


**Figure 9.** The cross-polar cap potential (CPCP) as a function of the IMF  $E_Y$  for the 2014 ICME cloud period, with nominal solar wind conditions before and after the ICME event taken into account separately. GUMICS-4 simulation data with 1 minute time resolution has been averaged by 10 minutes and binned by upstream  $E_Y$  with 0.5 mV/m intervals. Panels a, b and c are showing show the magnitudes of the IMF, the upstream flow speed and the Alfvén Mach number, respectively.

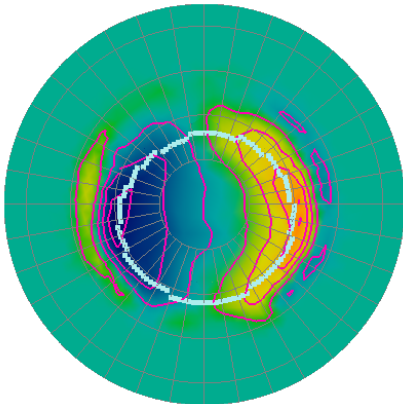
a) July 16, 01:00 0.5  $R_E$



b) July 16, 03:00 0.5  $R_E$



c) July 16, 01:00 0.25  $R_E$



d) July 16, 03:00 0.25  $R_E$

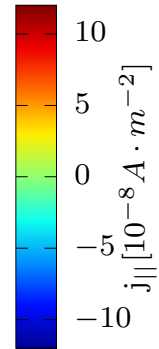
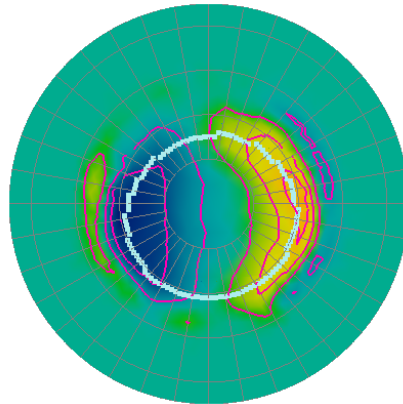


**Figure 10.** The [northern hemisphere](#) field-aligned current pattern in GUMICS-4 simulation at 01:00 UT (panels a and c) and at 03:00 UT (panels b and d) in July 16, 2012. Panels a and b (c and d) show the results of the simulation run in which 0.5 (0.25)  $R_E$  maximum spatial resolution was used.